Review

Wiley Online Library

ELECTROANALYSIS

DOI: 10.1002/elan.202100192

Application of MXene in Electrochemical Sensors: A Review

Xinzhao Wu,[a, b] Pinyi Ma,*[a] Ying Sun,[a] Fangxin Du,[b, c] Daqian Song,*[a] and Guobao Xu[b, c]

Abstract: Electroanalysis has obtained considerable progress over the past few years, especially in the field of electrochemical sensors. Broadly speaking, electrochemical sensors include not only conventional electrochemical biosensors or non-biosensors, but also emerging electrochemiluminescence (ECL) sensors and photoelectrochemical (PEC) sensors which are both combined with optical methods. In addition, various electrochemical sensing devices have been developed for practical purposes, such as multiplexed simultaneous detection of disease-related biomarkers and non-invasive body fluid monitoring. For the further performance improvement of electrochemical sensors, material is crucial. Recent years, a kind of two-dimensional (2D) nanomaterial MXene containing transition metal carbides, nitrides and carbonitrides, with unique structural, mechanical, electronic, optical, and thermal properties, have attracted a lot of attention form analytical chemists, and widely applied in electrochemical sensors. Here, we reviewed electrochemical sensors based on MXene from Nov. 2014 (when the first work about electrochemical sensor based on MXene published) to Mar. 2021, dividing them into different types as electrochemical biosensors, electrochemical non-biosensors, electrochemiluminescence sensors, photoelectrochemical sensors and flexible sensors. We believe this review will be of help to those who want to design or develop electrochemical sensors based on MXene, hoping new inspirations could be sparked.

Keywords: Electrochemical Sensors · Electrochemiluminescence · Photoelectrochemistry · Two-dimensional Materials · MXene

1 Introduction

Electroanalysis has a long history more than 200 years [1]. To the present day, it is electrochemical sensors that give the opportunity for electroanalytical chemists to remain competitive in analytical chemistry [2]. Electrochemical sensors can be divided into non-biosensors and biosensors. Since electrochemical non-biosensors based on the electrocatalysis of the prepared modified electrodes are often bogged down in the deficiency mire of selectivity, electrochemical biosensors combining the sensitivity of electroanalytical methods with inherent bioselectivity of biological components are showing powerful capabilities in electroanalysis [3]. Electrochemical biosensors can be also divided into two main categories based on the nature of the biological recognition process i.e. biocatalytic sensors and affinity sensors [3]. Biocatalytic sensors incorporate biological components, such as enzymes, whole cells and tissue slices, to recognize the target analyte, producing electroactive species or some other detectable outcome. While affinity sensors use the selective and strong binding of biomolecules such as antibodies, membrane receptors, and oligonucleotides, to produce a measurable electrical signal with a target analyte.

Apart from conventional electrochemical non-biosensors or biosensors, electrochemiluminescence (ECL) sensors and photoelectrochemical (PEC) sensors as evolutionary electroanalysis methods have also obtained substantial progress [4]. Electrochemiluminescence, also referred to as electrogenerated chemiluminescence, is chemiluminescence triggered by electrochemical methods [4b]. In the ECL process, species generated at electrodes undergo high-energy electron-transfer reactions to form excited states and then emit light [4a]. ECL has now become a very powerful analytical technique widely used in the areas of immunoassay, food and water testing and biowarfare agent detection. As a reverse of ECL, PEC process refers to photon-to-electricity conversion resulting from charge separation and subsequent charge transfer after absorption of photons during illumination [4e]. Different from traditional electrochemical sensing, the light is employed as an excitation source while electrical signal is used for the readout in PEC sensing. Because of the different energy forms between the excitation source

[a] X. Wu, P. Ma, Y. Sun, D. Song
College of Chemistry,
Jilin Province Research Center for Engineering and Technology of Spectral Analytical Instruments,
Jilin University,
Qianjin Street 2699, Changchun, Jilin 130012, P.R. China
E-mail: mapinyi@jlu.edu.cn
songdq@jlu.edu.cn
[b] X. Wu, F. Du, G. Xu
State Key Laboratory of Electroanalytical Chemistry,
Changchun Institute of Applied Chemistry,
Chinese Academy of Sciences,
5625 Renmin Street, Changchun, Jilin 130022, P.R. China
[c] F. Du, G. Xu
University of Chinese Academy of Sciences,
Beijing 100049, P.R. China

and detection signal, PEC sensing possesses potentially higher sensitivity than conventional electrochemical and chemiluminescent methods [5] And compared with various optical techniques involving sophisticated and expensive equipment, electrochemical signal pattern endows PEC biosensor virtues like robustness, lower cost, simpler instrumentation, higher sensitivity and easier to miniaturize [6]. Therefore ECL and PEC sensing strategies both naturally have advantages such as low cost and simple instrumentation with higher sensitivity due to the reduced background that originated from the total separation and the different energy forms of the excitation and detection signals [4h]. Some latest developments in ECL and PEC sensors especially for bioanalysis are discussed by reviews [7].

With remarkable achievements in nanotechnology and nanoscience, various nanomaterials have been focused and applied in electrochemical sensors [8]. Among numerous nanomaterials, a kind of two-dimensional (2D) layered inorganic nanomaterial termed as MXene have recently attracted huge interests [9].

MXene, with a 2D layered structure, referred to transition metal carbides, nitrides and carbonitrides, up to now has expanded rapidly into a large family [10]. The discovery of mechanically exfoliated graphene in 2004 caused a sensation all over the world [11], and studies around graphene powerfully demonstrate that layered materials when thinned to its physical limits (with thickness of few layers and two or even one layers) will exhibit novel properties different from their bulk counterparts [12]. So when the first MXene Ti_3C_2 was discovered in 2011, a great deal of attention to this new kind of 2D nanomaterial was received from materials scientists. MXenes are usually produced by selective etching of the A element (mostly groups 13 and 14 element) from the MAX phases, such as Ti_2AlC, Ti_3AlC_2, and Ta_4AlC_3. The chemical composition of MXenes has a general formula $M_{n+1}X_nT_x$ ($n=1\sim3$), where M represents an early transition metal, X is C and/or N, and T_x refers to surface-terminating functional groups such as oxygen (O), hydroxyl (–OH) or fluorine (–F) derived from the etching synthesis process [13]. The name "MXene" was given to describe the similarities between this 2D material family and graphene but also to recognize the parent MAX phases [14]. By adopting different synthesis methods, generally divided into bottom-up approaches and top-down approaches, varieties of single or few layered MXenes with versatile chemistries can be obtained [15]. Up to now, more than 200 different MXenes with stable phases based on combinations of various transition metals such as Ti, Mo, V, Cr and their alloys with C and N are determined or predicted [16]. The distinct features of MXenes, such as high electrical conductivity, excellent hydrophilicity, good chemical stability, high surface areas,

Xinzhao Wu received his bachelor's degree of applied chemistry from North China Electric Power University (NCEPU), China, in 2020. And now he is pursuing his master's degree of analytical chemistry under the direction of professor Daqian Song in Jilin University (JLU). His current research interests include the electrochemiluminescence properties of gold nanoclusters (AuNCs) and the design of ECL immunosensors based on the two-dimensional nanomaterial MXene.

Pinyi Ma received his doctor's degree in 2017 from College of Chemistry, Jilin University (JLU), China. Now he is a senior engineer in JLU. His research area includes spectral analysis and electrochemiluminescence immunosensors.

Ying Sun received her doctor's degree in 2009 from College of Chemistry, Jilin University (JLU), China. Now she is a professor in JLU. Her research area includes spectral analysis and biosensors.

Fangxin Du obtained her BSc degree from Hefei University of Technology in 2017. Currently she is studying for her PhD degree under the guidance of Prof. Guobao Xu at the State Key Laboratory of Electroanalytical Chemistry, Changchun Institute of Applied Chemistry, Chinese Academy of Sciences and University of Science and Technology of China. Her research interests focus on chemiluminescence, electrochemiluminescence and clinical analysis.

Daqian Song received his doctor's degree in 2003 from College of Chemistry, Jilin University (JLU), China. Now he is the director of Jilin province research center for engineering and technology of spectral analytical instruments, and a professor of JLU. He has published more than 160 papers in SCI indexed journals, and they are mainly concerned with spectral analysis and chromatographic analysis.

Guobao Xu received his BSc, MSc, and PhD from Jilin University, Xiamen University, and Changchun Institute of Applied Chemistry, respectively. He did postdoctoral research at the University of Hong Kong, the Hong Kong Polytechnic University, and NTT/JST. His research interests involve electrochemiluminescence, chemiluminescence, biosensing, precise synthesis of nanomaterials, energy conversion and storage, and devices.

tunable and abundant surface functionalities, ease of synthesizing large quantities in water, environment-friendly characteristics as well as non-toxic nature, endow them brilliant application prospects in analytical chemistry [17], such as fluorometric sensing [18], piezoresistive sensing [19], and photothermal sensing [20], especially in electrochemical sensing.

MXene as a kind of conducitve two-dimensional nanomaterial with abundant surface chemistry is an ideal carrier for biomolecules like enzymes, antibodies or aptamers for the construction of electrochemical biosensors. Song, D. D. et al. [21] synthesized a Ti_3C_2 MXene/Au NPs composite to immobilize acetylcholinesterase (AChE) and fabricated a electrochemical biosensor to detect organophosphorus pesticides (OPs) methamidophos, getting a a low limit of detection (LOD) of 0.134 pM. Dong, H. et al. [22] used ultrathin layered ammoniated Ti_3C_2 (NH_2–Ti_3C_2) to immobilize antibodies for the fabrication of a sandwich-type immunosensor to detect cardiac troponin I with a LOD of 8.3 fg/mL. F. et al. [23] synthesized a nanocarrier of the complementary DNA toward miRNA-155 on the basis of the nanohybrid type of $Ti_3C_2T_x$ MXene nanosheets decorated using iron phthalocyanine quantum dots and constructed an miRNA-155 impedimetric aptasensing system with a LOD of 4.3 aM. It is similar for the application of MXene in ECL biosensors. But for PEC sensors and flexible sensors, MXene is usually used for a component of heterojunctions or conductive films with better electronic performance and catalytic activity [24]. The detail will be discussed in corresponding chapters.

In a word, we will comprehensively review electrochemical sensors based on MXene from Nov. 2014 (when the first work about electrochemical sensor based on MXene was published) to Feb. 2021 dividing them into different types here, as electrochemical biosensors, electrochemical non-biosensors, electrochemiluminescence sensors, photoelectrochemical sensors and flexible sensors.

2 Unique Characteristics of MXene

The unique characteristics of MXene (Ti_3C_2 is the mostly used MXene) compared to other 2D materials make it be increasingly utilized in the construction of electrochemical sensors. These unique characteristics can be summarized as follows.

1. MXene has an obvious advantage of high electrical conductivity which is crucial for accelerating the heterogeneous electron transfer rate in comparison with other 2D materials. This excellent conductivity property is one of the most important bases for it to be applied in electrochemical sensors.
2. It is easy to synthesize MXene with a satisfactory solution dispersibility and stability. This is crucial for the fabrication of electrochemical sensors because the most used approach for the preparation of modified electrodes is drop-casting which requires preparation in advance of the well dispersed coating solution.
3. MXene is a powerful substrate material as inks for printing applications [25]. The printing and pre/post-patterned coating methods represent a whole range of simple, economically efficient, versatile, and eco-friendly manufacturing techniques for devices. Printing can allow for complex 3D architectures and multi-functionality that are highly required in various applications. Therefore, with the introduction of MXene, printing/coating could be developed toward a more powerful device fabrication tool as well as for industrialization.
4. Based on its high stretch ability and biocompatibility, MXene can be a powerful substrate for the fabrication of flexible conductive platforms that can be used to develop wearable electrochemical sensors [26], which are urgently required for health care monitoring and clinical analysis.
5. The 2D layered structure and the unique surface with abundant chemical groups give MXene a strong potential to be combined with a variety of functional materials or biomolecules for different analytical purposes. Various MXene-based nanostructures exhibited different and colorful properties [27] which are conductive to the design of electrochemical sensors or devices with different functions, especially to the new-type ECL or PEC sensors.
6. The biocompatibility of MXene with biomolecules like enzymes, proteins and nucleic acids and especially the non-toxic nature make it excellent carrier in biosensors or biomedical applications.
7. The unique photothermal conversion ability of MXene make the dual-model detection strategy possible in the design of electrochemical sensors [28] which broaden the signal strategies of electrochemical sensors.

3 Application of MXene in Electrochemical Sensors

The unique characteristics of MXene render it promising material for electrochemical sensors. And with the increasing attention to MXene, we can say that the application of MXene in electrochemical sensors is in the ascendant. Now, we will review electrochemical sensors based on MXene from Nov. 2014 to Mar. 2021 dividing them into different types, as electrochemical biosensors, electrochemical non-biosensors, electrochemiluminescence sensors, photoelectrochemical sensors and flexible sensors. We will not introduce every work, but these MXene based electrochemical sensors are all listed in the Table 1. and Table 2.

3.1 Electrochemical Biosensors

3.1.1 Enzyme-based Biosensors

Direct electron transfer (DET) between enzymes and electrodes is cardinal for the construction of electro-

Table 1. Electrochemical sensors based on MXene from Nov. 2014 to Dec. 2019 (31 articles).

Analytes	Materials	Electrochemical Methods	LODs	Dynamic Ranges
H_2O_2 [29]	Ti_3C_2	Amperometric (i-t) Method	20 nM	0.1–260 μM
H_2O_2 [30]	Ti_3C_2/TiO_2	Amperometric (i-t) Method	14 nM	0.1–380 μM
H_2O_2 [31]	Ti_3C_2/graphene oxide (GO)	Differential Pulse Voltammetry	1.95 μM	2 μM–1 mM
H_2O_2 [32]	Ti_3C_2/NiO	Differential Pulse Voltammetry	0.34μM	10μM–4.5mM
glucose [33]	Ti_3C_2/AuNPs	Amperometric (i-t) Method	5.9 μM	0.1–18 mM
glucose [34]	Ti_3C_2/NiCo layered double hydroxide (LDH)	Amperometric (i-t) Method	0.53μM	0.002–4.096mM
glucose [35]	Ti_3C_2/Cu_2O	Photoelectrochemical Method	0.17 nM	0.5nM–0.5mM
NO_2^- [36]	Ti_3C_2/AuNPs	Amperometric (i-t) Method	0.14 μM	1.0–4581.1 μM
NO_2^- [37]	Ti_3C_2	Amperometric (i-t) Method	0.12 μM	0.5–11800 μM
BrO_3^- [38]	Ti_3C_2	Differential Pulse Voltammetry	41 nM	50nM–5μM
$O_2^{\bullet -}$ [39]	$Ti_3C_2/Mn_3(PO_4)_2$	Amperometric (i-t) Method	0.5 nM	2.5 nM–14 μM
dopamine [40]	Ti_3C_2/PtNPs/PdNPs	Amperometric (i-t) Method	30nM	0.2–1000μM
dopamine [41]	Ti_3C_2	Amperometric (i-t) Method	3 nM	0.015–10 μM
malathion [42]	Ti_3C_2	Differential Pulse Voltammetry	0.003 pM	0.01 pM–0.01 μM
malathion [43]	Ti_3C_2/AgNPs	Differential Pulse Voltammetry	0.00327 pM	0.01 pM–0.01 μM
methamidophos [44]	$Ti_3C_2/(MnO_2/Mn_3O_4)$/AuNPs	Differential Pulse Voltammetry	0.134 pM	1 pM–1 μM
carbendazim (CBZ) [45]	Ti_3C_2	Differential Pulse Voltammetry	10.3 nM	50nM–100μM
carbendazim (CBZ) [46]	Ti_3C_2/electrochemically reduced graphene oxide (ERGO)	Differential Pulse Voltammetry	0.67 nM	2.0 nM–10.0 μM
Acetaminophen (ACOP) isoniazid (INZ) [47]	Ti_3C_2	Differential Pulse Voltammetry	ACOP 0.048μM INZ 0.064mM	ACOP 0.25–2000Mm INZ 0.1–4.6mM
phenol [48]	Ti_3C_2	Amperometric (i-t) Method	12 nM	0.05–15.5 μM
inosine monophosphate (IMP) [49]	Ti_3C_2/Au@Pt nanoflowers	Amperometric (i-t) Method	2.73 ng/mL	0.04–17 g/L
lactate [50]	Ti_3C_2/PtNPs	Amperometric (i-t) Method	5.0 μM	0.005–5.0 mM
adrenaline [51]	Ti_2C	Amperometric (i-t) Method	9.5 nM	0.02–100 μM
piroxicam [52]	Ti_3C_2/methylene blue (MB)/CuNPs	Square Wave Voltammetry	0.05 μM	0.1–80 μM
L-cysteine (L–Cys) [53]	Ti_3C_2/PdNPs	Amperometric (i-t) Method	0.14 μM	0.5–10 μM
catechol (CT) hydroquinone (HQ) [54]	Ti_3C_2/multi-walled carbon nanotubes (MWCNTs)	Differential Pulse Voltammetry	HQ 3.9nM CT 6.6nM	both 2–150μM
prostate-specific antigen (PSA) [55]	Ti_3C_2	Capacitance Method	0.031ng/mL	0.1ng/ml–50ng/mL
osteopontin (OPN) [56]	polypyrrole (PPy)@(Ti_3C_2/phosphomolybdic acid (PMo_{12}))	Impedimetric Method	0.98 fg/mL	0.05–10,000pg/mL
single-nucleotide mismatch detection [57]	Ti_3C_2	Electrochemiluminescence	~	~
MCF-7 exosomes [58]	Ti_3C_2	Electrochemiluminescence	125 particles/μL	5×10^2–5×10^6 particles/μL
glutathione [59]	Ti_3C_2 quantum dots (QDs)/TiO_2 inverse opal photonic crystals (IOPCs)	Photoelectrochemical Method	0.55 μM	0.1–1000 μM

Table 2. Electrochemical sensors based on MXene from Jan. 2020 to Mar. 2021 (48 articles).

Analytes	Materials	Electrochemical Methods	LODs	Dynamic Ranges
Enzyme-based Biosensors				
Glucose [60]	Ti_3C_2	Cyclic Voltammetry	2.6 μM	0.02–1.1; 4.0–20 mM
Glucose [61]	Ti_3C_2	Amperometric (i-t) Method	23.0 μM	50-27750 μM
Phosmet [62]	Nb_2C	Amperometric (i-t) Method	0.046 ng/mL	200×10^{-12}–$\times10^{-6}$ M
Paraoxon [63]	Ti_3C_2/Au-PdNPs	Amperometric (i-t) Method	1.75 ng/L	0.1–1000 μg/L
β-hydroxybutyrate [64]	Ti_3C_2	Amperometric (i-t) Method	45 μM	0.36 to 17.9 mM
Immunosensors				
Cardiac Troponin I [22]	CuPtRh/NH_2-Ti_3C_2	Amperometric (i-t) Method	8.3 fg/mL	25 fg/mL—100 ng/mL
Procalcitonin [65]	Ti_3C_2/AuNPs	Differential Pulse Voltammetry	2.0 fg/mL	0.01–1.0 pg/mL
Prostate Specific Antigen [66]	Ti_3C_2/AuNPs	Differential Pulse Voltammetry	3.0 fg/mL	0.01–1.0 pg/mL
Aptasensors				
microRNA-155 [23]	Ti_3C_2/FePcQDs	Impedimetric Method	4.3 aM	0.01 fM–10 pM
microRNA-155 [67]	AuNPs/Ti_3C_2	Differential Pulse Voltammetry	0.35 fM	1.0 fM to 10 nM
Mycobacterium tuberculosis [68]	Ti_3C_2	Conductometry	20 CFU/mL	~
Mucin1 (MUC1) [69]	Ti_3C_2	Square Wave Voltammetry	0.33 pM	1.0 Pm–10 mM
Exosomes [70]	Ti_3C_2	Square Wave Voltammetry	229 particles/μL	500 particles/μL to 500000 particles/μL
Thyroxine (T4) [71]	Ti_3C_2/MoS_2	Differential Pulse Voltammetry	0.39 pg/mL	0.7 to 7800000 pg/mL
Electrochemical Non-biosensors				
Carbendazim [72]	Ti_3C_2/CNHs/β-CD-MOFs	Differential Pulse Voltammetry	1.0 nM	3.0 nM–10.0 μM
Catechol (CT) Hydroquinone (HQ) [73]	alk-Ti_3C_2/N-PC	Differential Pulse Voltammetry	CT 3.1 nM HQ 4.8 nM	0.5 μM–150 μM
H_2O_2 [74]	Ti_3C_2/PBNPs	Amperometric (i-t) Method	0.20 μM	0.6–63.6 μM; 63.6–254 μM
Fisetin [75]	Ti_3C_2/NH_2-CNTs	Differential Pulse Voltammetry	1.0 nM	0.003 μM–20.0 μM
Furazolidone [76]	VC/g-CN	Amperometric (i-t) Method	0.5 nM	0.004–141 μM
Sulfadiazine [77]	Ti_3C_2/BN	Differential Pulse Voltammetry	3.0 nM	0.01–44; 59–186 μM

Table 2. continued

Analytes	Materials	Electrochemical Methods	LODs	Dynamic Ranges
Enzyme-based Biosensors				
Ifosfamide (IFO) Acetaminophen (ACOP) Domperidone (DOM) Sumatriptan (SUM) [78]	Ti_3C_2/MWCNT	Adsorptive Stripping Differential Pulse Voltammetry	IFO 0.00031 μM ACOP 0.00028 μM DOM 0.00034 μM SUM 0.00042 μM	IFO 0.0011–1.0 μM ACOP 0.0042–7.1 μM DOM 0.0046–7.3 μM SUM 0.0033–61 μM
Uric acid (UA) Folic acid (FA) [79]	Ti_3C_2/AuNPs	Amperometric (i-t) Method	UA 11.5 nM FA 6.20 nM	UA 0.03–1520 μM FA 0.02–3580 μM
NO_2^- [80]	Ti_3C_2/TiO_2	Differential Pulse Voltammetry	0.85 μM	0.003 to 0.25 mM and 0.25 to 1.25 mM
NO_2^- [81]	Ti_3C_2/AuNPs	Amperometric (i-t) Method	0.059 μM	0.1–2490 μM and 2490–13490 μM
Pb^{2+} Cd^{2+} [82]	Ti_3C_2/BiNPs	Square Wave Stripping Voltammetry	Pb^{2+} 10.8 nM Cd^{2+} 12.4 nM	Pb^{2+} 0.06 to 0.6 μM Cd^{2+} 0.08 to 0.6 μM
Pb^{2+} Cd^{2+} [83]	Ti_3C_2/protonated carbon nitride (H–C_3N_4)	Square Wave Stripping Voltammetry	Pb^{2+} 0.6 nM Cd^{2+} 1 nM	0.05–1.50 μM
Pb^{2+} [84]	$Nb_4C_3T_x$	Square Wave Stripping Voltammetry	12 nM	0.025–0.5 μM
4-nitroquinoline N-oxide (4-NO) [85]	TiC	Differential Pulse Voltammetry	2 nM	0.01–114 μM and 133–650 μM
Hydrazine [86]	Ti_3C_2/ZIF-8	Amperometric (i-t) Method	5.1 μM	10 μm to 7.7 mM
Dopamine [87]	Nb_2C/ZnS	Differential Pulse Voltammetry	1.39 μM	0.09–0.82 mM
Electrochemiluminescence Sensors				
Carcinoembryonic Antigen [88]	Ti_3C_2/AuNPs	Electrochemiluminescence	34.58 fg/mL	0.1 pg/mL–10ng/mL
Exosomes [28]	Ti_3C_2/BPQDs	Electrochemiluminescence	37.0 particle/μL	1.1×10^2 particle/μL–1.1×10^7 particle/μL
Thyroglobulin [89]	Nb_2CT/ZnOQDs	Electrochemiluminescence	~1 fg/mL	1 fg/mL–10 ng/mL
Exosomes [90]	Ti_3C_2/AuNPs	Electrochemiluminescence	30 particle/μL	10^2 particle/μL–10^5 particle/μL
Mucin 1 (MUC1) [91]	Ti_3C_2/Ru	Electrochemiluminescence	26.9 ag/mL	100 ag/mL to 10 ng/mL
Photoelectrochemical Sensors				
CD44 protein [92]	$TiO_2/Ti_3C_2/BiVO_4$	Photoelectrochemical Method	14 fg/mL	0.22 pg/mL–3.2 ng/mL
Antioxidants (such as ascorbic acid (AA)) [93]	TiO_2/Ti_3C_2	Photoelectrochemical Method	AA 1.2 μM	AA 12.48–521.33 μM
Glucose [24a]	$TiO_2/Ti_3C_2/Cu_2O$	Photoelectrochemical Method	33.75 nM	100 nM–10 μM
Prostate-Specific Antigens [94]	$TiO_2/Ti_3C_2/NiWO_4$	Photoelectrochemical Method	0.15 fg/mL	1.2 fg/mL–0.18 mg/mL
Ciprofloxacin (CFX) [95]	Ti_3C_2/g-C_3N_4	Photoelectrochemical Method	0.13 nM	0.4 to 1000 nM

Table 2. continued

Analytes	Materials	Electrochemical Methods	LODs	Dynamic Ranges
Enzyme-based Biosensors				
H^{g2+} [96]	$Ti_3C_2/BiVO_4$	Photoelectrochemical Method	1 pM	1 pM to 2 nM
Flexible Electrochemical Sensors and Others				
Apo-A1 and NMP 22 [97]	Ti_3C_2	Differential Pulse Voltammetry	Apo-A1 0.3 pg/mL NMP 22 0.7 pg/mL	0.1 pg/mL–50 ng/mL
$O_2^{\bullet-}$ [98]	Ti_3C_2/AuPtNPs	Amperometric (i-t) Method	0.2 μM	0.4–9.5 μM
$O_2^{\bullet-}$ [99]	$Ti_3C_2/Mn_3(PO_4)_2$	Amperometric (i-t) Method	1.63 nM	5.75 nM–25.93 μM
Copper (Cu) and Zinc (Zn) ions [24b]	Ti_3C_2/MWCNTs	Square Wave Anodic Stripping Voltammetry	Cu 0.1 ppb Zn 1.5 ppb	Cu 10–500 ppb Zn 200–600 ppb
K^+ [100]	Ti_3C_2/MWCNTs	Potentiometric Method	Sensitivity 173 mV/dec	1–32 mM
miR-21 and miR-141 [101]	Ti_3C_2/AuNPs	Differential Pulse Voltammetry	miR-21 204 aM miR-141 138 aM	500 aM-50 nM
Glucose and Lactate [102]	Ti_3C_2	Amperometric (i-t) Method	Glucose 17.05 μM Lactate 3.73 μM	Glucose 0.08–1.25 mM Lactate 0.3–20.3 mM

chemical biosensors [61]. MXene possess numerous distinct properties, for instance large specific surface area and outstanding electrical conductivity, therefore the introduction of MXene could possibly be as an efficient pathway to facilitate DET [61]. Ti_3C_2 is the first MXene to be applied in the fabrication of electrochemical sensors, and the first electrochemical sensor based on Ti_3C_2 is an enzyme-based biosensor fabricated in 2014 for the detecton of H_2O_2 [29]. The Ti_3C_2 MXene was used to immobilize the enzyme hemoglobin (Hb) which not only showed good enzyme immbilization ability but also provided a favorable microenvironment for the protein to retain its activity and stability. Moreover, the direct electron transfer of Hb was facilitated, demonstrating that immobilizing enzymes onto the surface of Ti_3C_2 MXene is an efficient way to fabricate mediator-free enzyme-based biosensors. Attempts to immobilize other enzymes like acetylcholinesterase (AChE) [103] and tyrosinase [104] onto the surface of Ti_3C_2 MXene were also conducted. Their works indicated that Ti_3C_2 MXene with large specific surface area, good biocompatibility, hydrophilic surface and excellent metallic conductivity is indeed a good candidate as an excellent immobilization matrix for fabricating enzyme-based biosensors.

To further improve the performance of enzyme-based biosensors based on Ti_3C_2 MXene, the strategy of combining Ti_3C_2 MXene with other functional materials especially various nanomaterials into composite has been adopted by many researchers. For example, TiO_2 nanoparticles (NPs) were modified on the Ti_3C_2 MXene by Wang, F. et al. to further enhance the active surface area available for protein adsorption, and retain enzymatic stability and activity [105]. Their fabricated Hb-based biosensor exhibited a better detection performance toward H_2O_2 with the limit of detection (LOD) of 14 nM compared to the one without TiO_2NPs. Besides, a glucose oxidase (GOx)-based biosensor based on Au/Ti_3C_2 MXene nanocomposite was fabricated by Rakhi, R. B. et al. for the detection of glucose [33]. The introduction of Au NPs bring the Au/Ti_3C_2 MXene nanocomposite with unique electrocatalytic properties due to their synergistic effects. And the prepared GOx/AuNPs/Ti_3C_2/Nafion/GCE biosensor displayed a relatively high amperometric sensitivity of 4.2 $\mu A m M^{-1} cm^{-2}$ and a LOD of 5.9 μM toward glucose. Also, Zhou, L. Y. et al. [106] used an Ag@Ti_3C_2 nanocomposite as nanocarrier for AChE and fabricated a malathion biosensor. Song, D. D. et al. [21] also fabricated a AChE-based biosensor for the determination of organophosphorus pesticides (OPs) methamidophos. Their biosensor was based on a three-dimensional (3D) MnO_2/Mn_3O_4/MXene/AuNPs composite (Figure 1) possessing a low LOD of 0.134 pM toward methamidophos. Wang, G. X. et al. [107]. assembled a dual-enzyme biosensor for the detection of inosine monophosphate (IMP). In their work, Ti_3C_2 MXene was combined with Au@Pt nanoflowers to obtain a good catalytic ability, and then with two enzymes (5′-nucleotidase and xanthine oxidase) immobilized on. The prepared biosensor showed

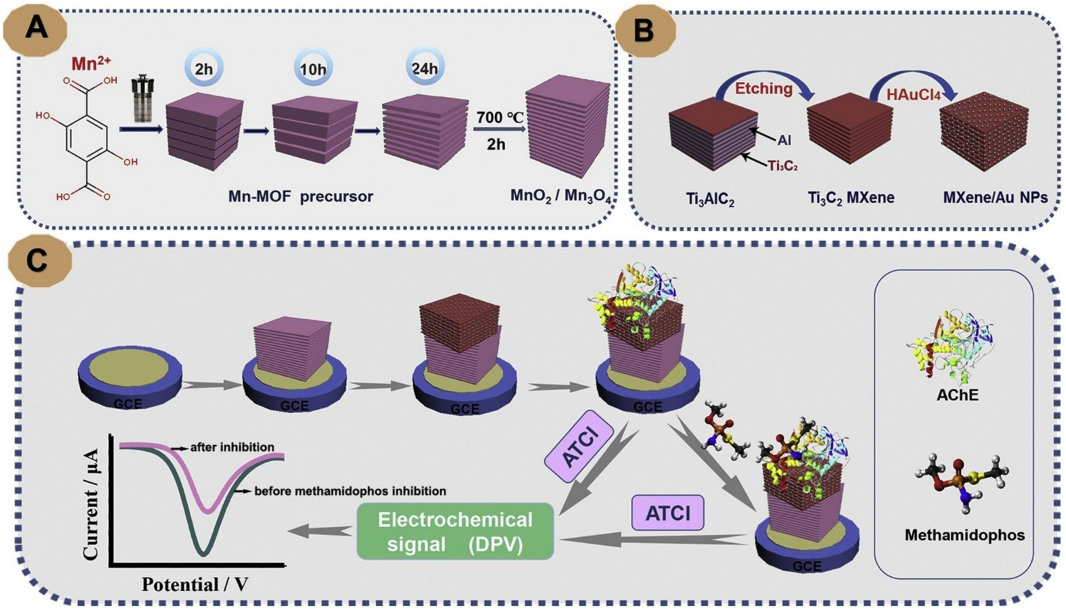

Fig. 1. Illustration of the formation of MnO_2/Mn_3O_4 composite (A), MXene/Au NPs (B), the fabrication process of AChE-Chit/MXene/AuNPs/MnO_2/Mn_3O_4/GCE biosensor for methamidophos assay. (Reprinted from [21] with permission: © 2019 Elsevier B.V.)

a LOD of 2.73 ng/mL toward inosine monophosphate in meat

For glucose biosensing, the toxic intermediate product (H_2O_2) generated during the enzymatic glucose oxidation often inhibits the activity of GOx in practical applications [60]. To tackle this issue, Wu, M. et al. [60] developed a hybrid Ti_3C_2/poly-L-lysine (PLL)/glucose oxidase (GOx) nanoreactor (Figure 2) that could catalyze the cascade reactions of glucose oxidation and the intermediate H_2O_2 decomposition. The Ti_3C_2 MXene was found having the ability to catalyze the decomposition reaction of H_2O_2, and with the loaded GOx a cascade reaction in glucose decomposition was formed. The Ti_3C_2/PLL/GOx nanoreactors with superior catalytic performance were deposited on glassy carbon electrode to construct a glucose biosensor with a LOD of 2.6 μM.

Conventional HF etching synthesis method of MXenes may bring some obstructions for their biosensing applications [62]. For example, due to excessive use of HF acid

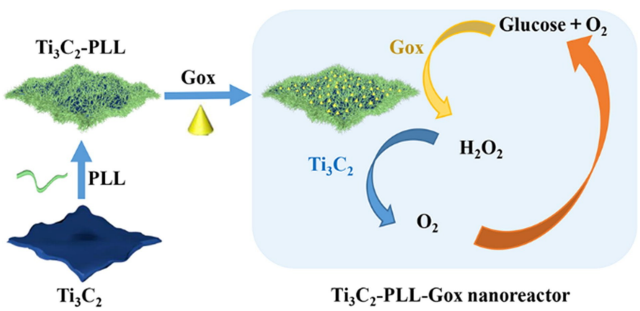

Fig. 2. Schematic illustration of the Ti_3C_2-PLL-GOx nanoreactor. (Reprinted from [60] with permission: © 2020 Elsevier Inc.)

the F^- residues on the surface of MXenes are prone to release HF during the hydrolysis reactions or electrochemical reactions, and the potential toxicity of HF would relatively reduce the enzyme activity or cause a significant damage to the normal cells in vivo. Also, HF-etched MXenes are susceptible to oxidation under ambient environment or during the oxygen evolution reaction (OER) process, severely affecting the stability and effectiveness of MXenes in biosensing process. Therefore, safe, robust, and fluorine-free synthesis methods for producing stable and biocompatible MXene nanosheets are essentially required. Song, M. et al. [62] constructed a fluoride-free Nb_2C/acetylcholinesterase (AChE)-based biosensor for the detection of phosmet. They synthesized the 2D fluoride-free Nb_2C MXene nanosheets through an electrochemical etching (E-etching) exfoliation route (Figure 3) and the obtained fluoride-free Nb_2C showed good chemical stability, low cytotoxicity, high porosity, large surface area and enhanced conductivity which were beneficial to the stabilization of enzyme activity and the promotion of electrochemical activity. The constructed Nb_2C/AChE-based biosensor realized a LOD down to 144×10^{-12} M (0.046 ng/mL) for phosmet. In the meantime, their work also showed that Nb_2C based biosensor system outperformed the counterpart of V_2C and Ti_3C_2 due to its excellent metallic properties with near-zero energy bandgap. Expect for the above, Zhao, F. et al. [63] proposed a disposable electrochemical AChE-based biosensor for the detection paraoxonin, using nanocomposites Ti_3C_2/Au–Pd as the functional platform. They prepared bimetallic nanoparticles (Au–Pd NPs) by self-reduction on the surface of ultrathin Ti_3C_2 nanosheets. With the combination of disposable screen-printed electrode (SPE) the fabricated AChE-based biosensor ex-

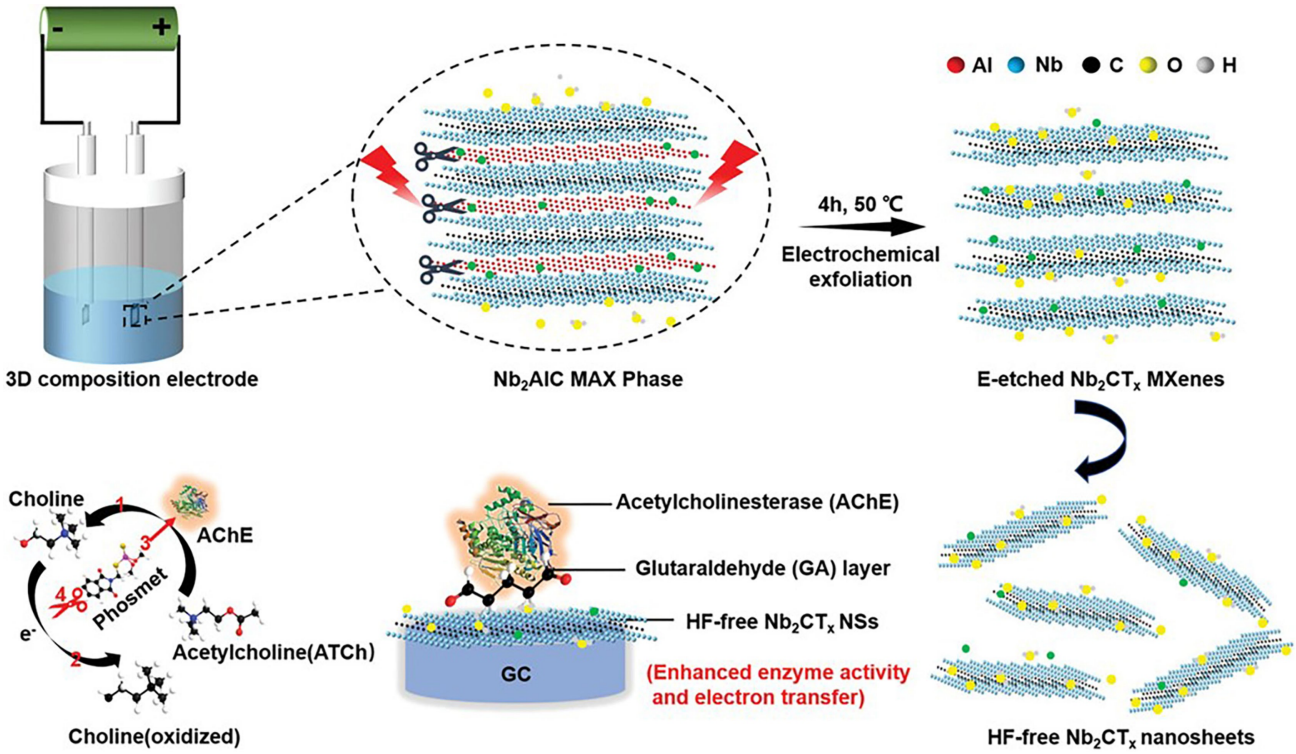

Fig. 3. Schematic for exfoliation and delamination process of Nb_2AlC MAX phase via electrochemical etching and the enzyme inhibition effect for phosmet detection by HF-free Nb_2CT_x/AChE based biosensor. (Reprinted from [62] © 2020 The Authors. Published by Wiley-VCH GmbH).

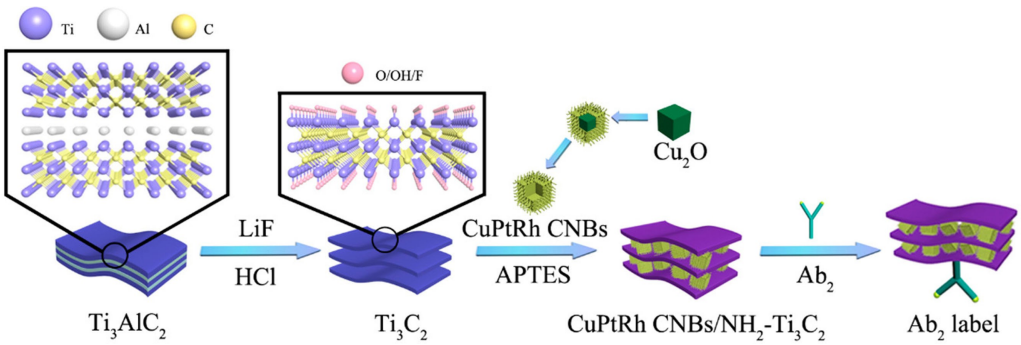

Fig. 4. Preparation of the CuPtRh/NH_2-Ti_3C_2 Ab_2 label. (Reprinted from [22] with permission: © 2019 American Chemical Society).

hibited a dynamic range from 0.1 to 1000 µg/L, as well as a low LOD of 1.75 ng/L. The AChE-based biosensor was successfully applied for paraoxon detection in pear and cucumber samples.

Ti_3C_2 MXene can also be developed to be a component of conductive substrate in other electrode systems apart from glassy carbon electrode (GCE). A Ti_3C_2/graphene oxide (Ti_3C_2–GO) nanocomposite was synthesized and applied for the fabrication of inkjet-printed hydrogen peroxide (H_2O_2) biosensor [31]. Their work demonstrated that the printable Ti_3C_2–GO nanocomposite was an excellent sensing platform for electrochemical determination. Besides, a nanocomposite consisting of platinum particles, polyaniline and Ti_3C_2 MXene (Pt/PANI/MXene) was used to modify a screen-printed carbon electrode (SPCE) to obtain the biosensor for both hydrogen peroxide and lactate [50]. The prepared SPCE provided a LOD of 1.0 µM toward H_2O_2. And after lactate oxidase immobilization, the lactate assay was performed by amperometry obtaining a LOD of 5.0 µM toward lactate. The biosensor could be used for the determination of lactate in milk samples with high stability and reliability.

3.1.2 Immunosensors

The earliest immunosensor based on MXene was fabricated in 2019 for the detection of prostate-specific antigen

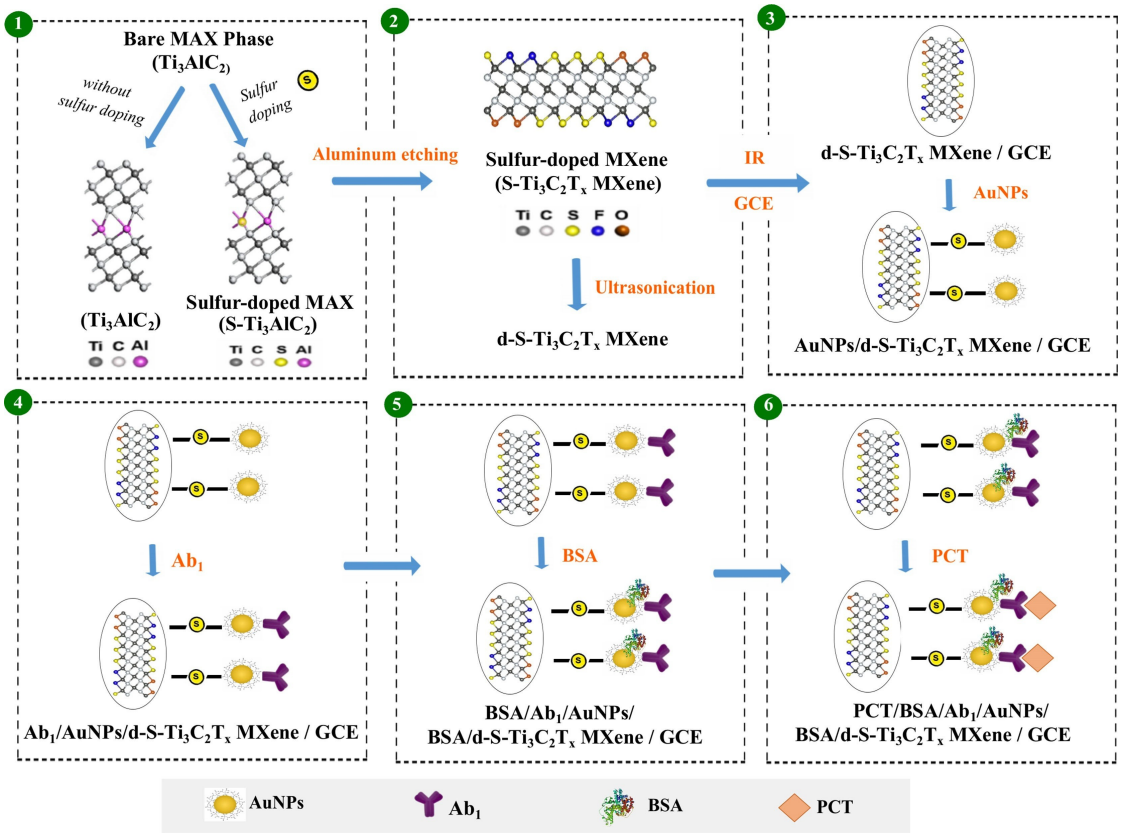

Fig. 5. Preparation procedure of PCT/BSA/Ab_1/AuNPs/d-S-$Ti_3C_2T_X$ MXene/GCE. (Reprinted from [65] with permission: © 2020 Elsevier B.V.)

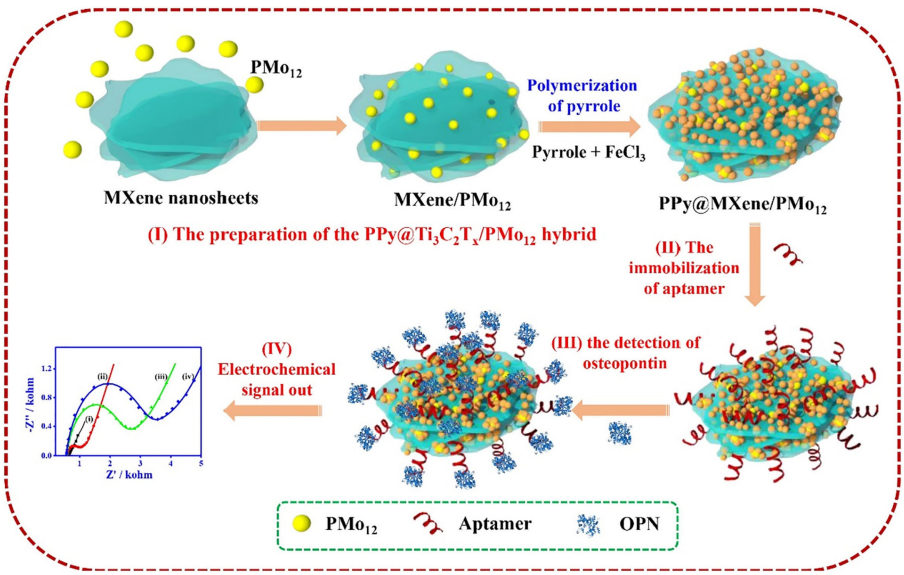

Fig. 6. Schematic diagram of the aptasensor fabrication based on PPy@$Ti_3C_2T_x$/PMo_{12} for the OPN detection, including (I) the preparation of the PPy@$Ti_3C_2T_x$/PMo_{12} hybrid, (II) the aptamer immobilization, (III) the OPN detection, and (IV) the electrochemical signal out. (Reprinted from [56] with permission: © 2019 Elsevier B.V.)

(PSA) [108]. Then, Dong, H. et al. [22] fabricated a sandwich-type immunosensor for the detection of cardiac troponin I with the use of a nanocomposite (CuPtRh/NH_2-Ti_3C_2) consisting of trimetallic hollow CuPtRh cubic nanoboxs (CuPtRh CNBs) and few layered ultrathin ammoniated Ti_3C_2 (NH_2–Ti_3C_2) (Figure 4). NH_2–Ti_3C_2

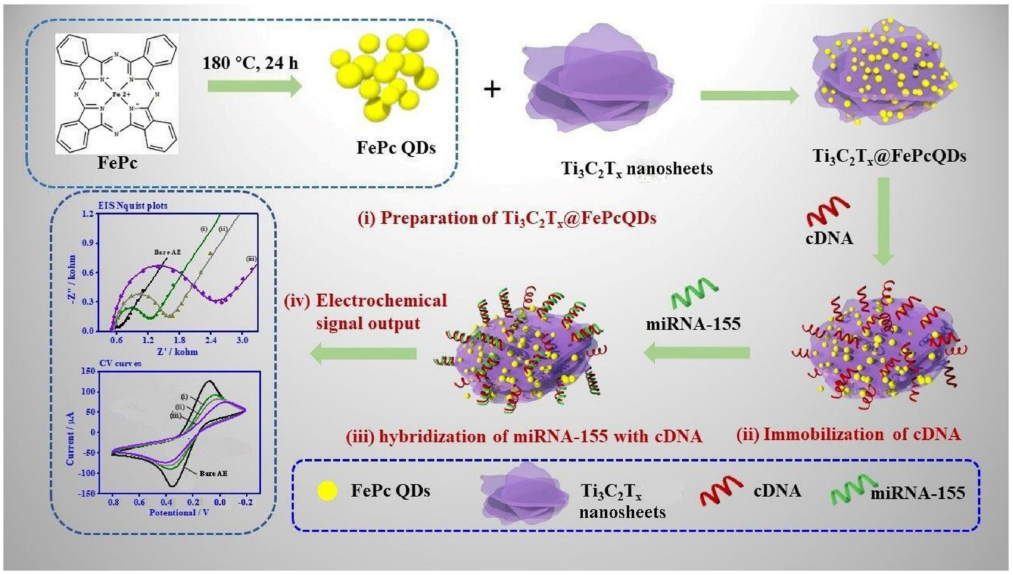

Fig. 7. Schematic diagram of the $Ti_3C_2T_x$@FePcQDs-based aptasensor for detecting miRNA-155, including (i) the preparation of $Ti_3C_2T_x$@FePcQDs nanohybrids, (ii) the immobilization of aptamer, (iii) the hybridization of miRNA-155 with cDNA, and (iv) different electrochemical signal output. (Reprinted from [23] with permission: © 2020 Elsevier B.V.)

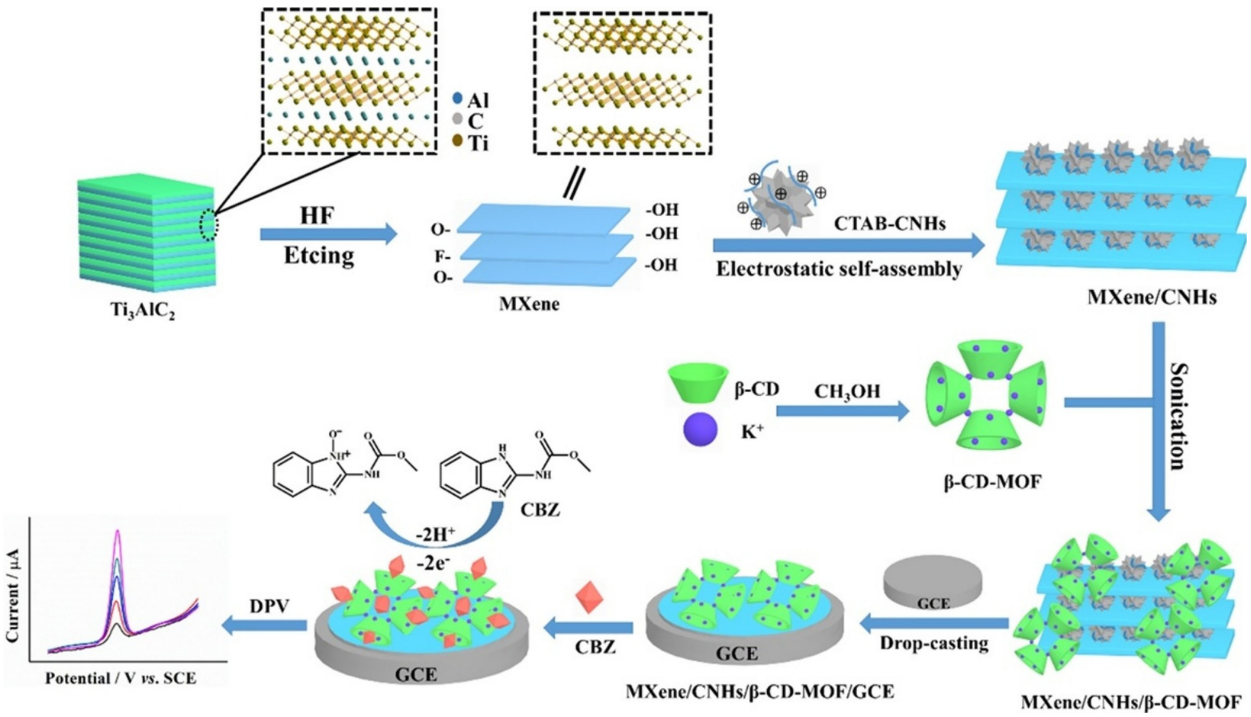

Fig. 8. Synthetic route of MXene/CNHs/β-CD-MOFs and the sensing strategy for CBZ. (Reprinted from [72] with permission: © 2020 Elsevier B.V.)

was selected as support material for CuPtRh CNBs and the secondary antibodies (Ab_2), and the prepared CuPtRh CNBs embedded in NH_2-Ti_3C_2 acted not only as a spacer to prevent the NH_2–Ti_3C_2 layer from irreversibly restacking but also as a connector to fix more Ab_2, through stable Pt–N and Rh–N bonds. The CuPtRh CNBs/NH_2–Ti_3C_2 as an Ab_2 label possessed high catalytic activity to the reduction of H_2O_2 therefore significantly amplifying the immunosensor's signal. The designed immunosensor showed a LOD of 8.3 fg/mL. Also for the detection of PSA, Medetalibeyoglu, H. et al. [66] utilized a self-assembled delaminated MXene-gold nanoparticles (d-$Ti_3C_2T_X$ MXene@AuNPs) composite to label PSA Ab_2 as

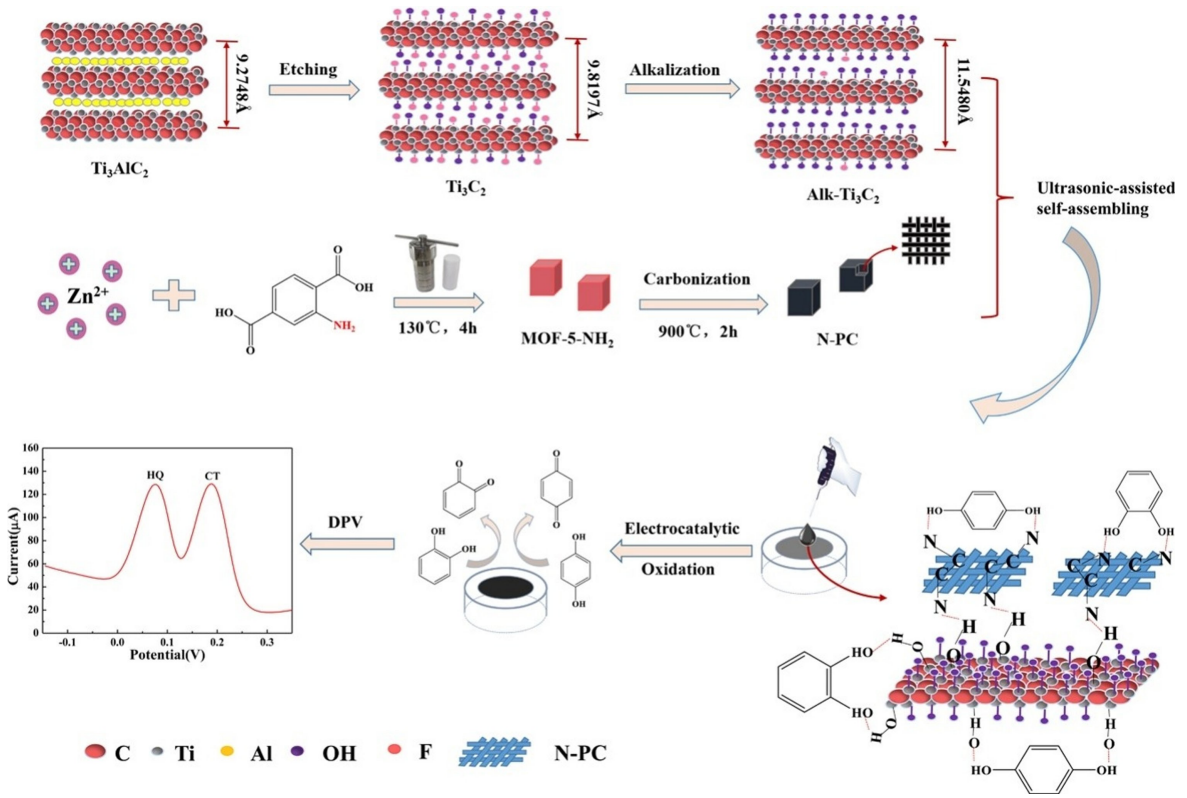

Fig. 9. Schematic illustration of the preparation and application of alk-Ti_3C_2/N-PC/GCE. (Reprinted from [73] with permission: © 2020 Elsevier B.V.)

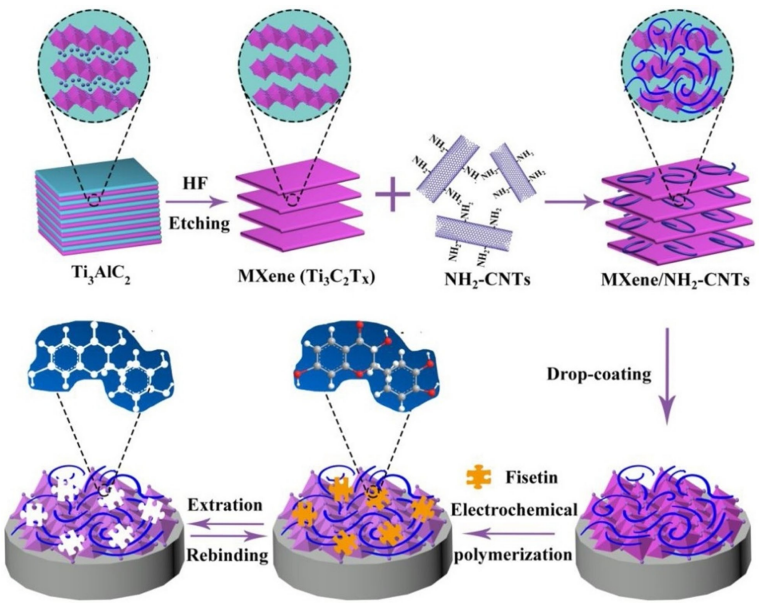

Fig. 10. Schematic illustration for the preparation of MIP/MXene/NH2-CNTs/GCE and the adsorption mechanism in the imprinted cavity. (Reprinted from [75] with permission: © 2020 Elsevier B.V

signal amplification. The obtained LOD was 3.0 fg/mL better than the above mentioned one (31 pg/mL).

Besides, Medetalibeyoglu, H. et al. [65] constructed a sandwich type electrochemical immunosensor for the detection of procalcitonin (Figure 5). In their work, delaminated sulfur-doped MXene (d-S-Ti_3C_2 MXene) modified glassy carbon electrode (GCE) including AuNPs was utilized as immunosensor platform to increase the

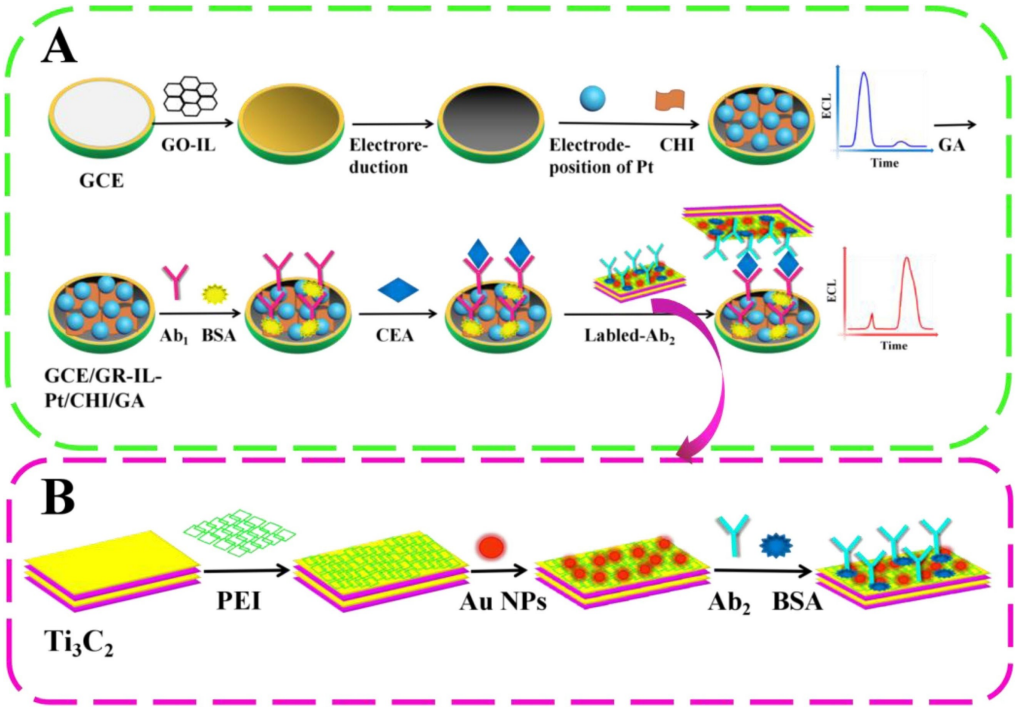

Fig. 11. The construction strategy of ratiometric ECL sensor (A); The preparation of the labled-Ab_2 (B). (Reprinted from [88] with permission: © 2020 Elsevier B.V.)

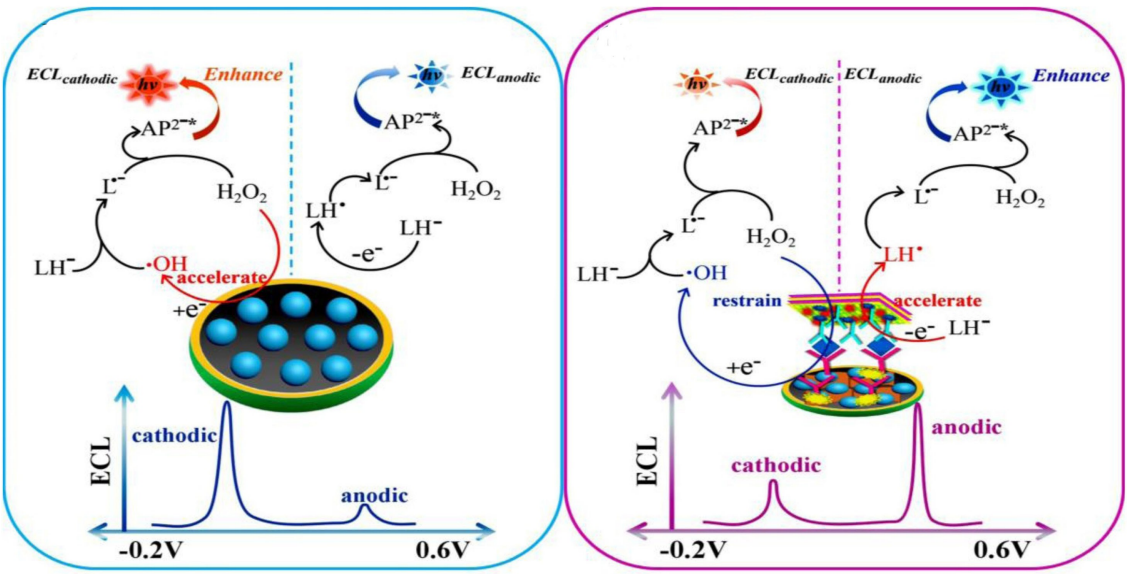

Fig. 12. The possible ECL mechanisms of the sensor without and with Ti_3C_2 MXenes-Au NPs–Ab2 nanoprobe. (Reprinted from [88] with permission: © 2020 Elsevier B.V.)

amount of PCT Ab_1, and carboxylated graphitic carbon nitride (c-g-C_3N_4) was used to label PCT Ab_2 as signal amplification.

3.1.3 Aptasensors

To date, thousands of DNA and RNA aptamers that bind to specific targets have been selected, including small molecules, proteins, peptides, bacteria, virus, and live cells [109]. And electrochemical aptasensors are widely explored due to the advantages of simplicity, fast response, low cost, recyclability, and miniaturization [110]. The first aptasensor based on MXene was constructed by anchoring RNA aptamers on the surface of a PPy@Ti_3C_2/PMo_{12} composite (PPy, polypyrrole; PMo_{12}, phosphomolybdic acid) to detect osteopontin (OPN) by an impedimetric

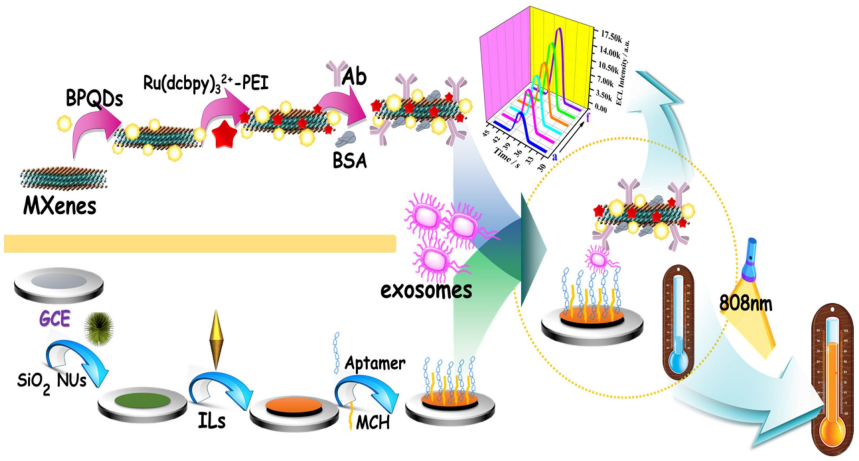

Fig. 13. Schematic illustration of the dual-mode biosensor for exosomes detection. (Reprinted from [28] with permission: © 2019 Elsevier B.V.)

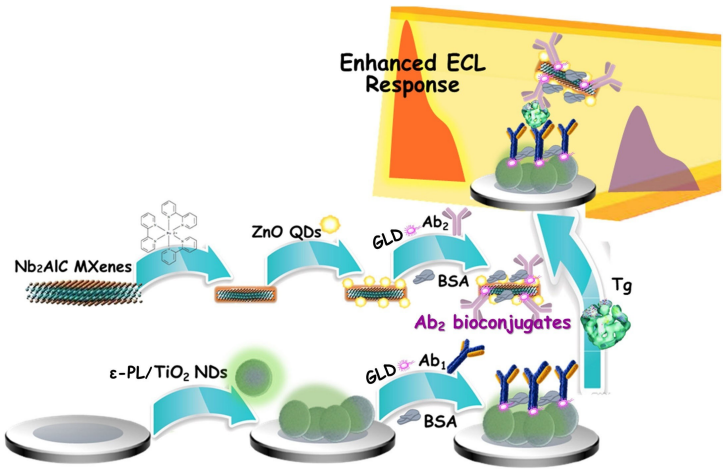

Fig. 14. Schematic illustration of the ECL immunosensor. (Reprinted from [89] with permission: © 2020 Elsevier B.V.)

method [56] (Figure 6). In the presence of OPN, the OPN aptamer strand immobilized over PPy@Ti_3C_2/PMo_{12} hybrid could form a G-quadruplex with OPN, hampering the used redox probes to access the electrode surface. Their aptasensor exhibited a low LOD of 0.98 fg/mL.

Also, Duan, F. et al. [23] developed an impedimetric aptasensor based on a novel zero dimensional (0D)/2D nanohybrid of Ti_3C_2 nanosheets decorated with Fe phthalocyanines quantum dots (FePc QDs) to sensitively detect miRNA-155 (Figure 7). The Ti_3C_2/FePcQDs nanohybrid acted as a nanocarrier for anchoring the complementary DNA (cDNA)-targeted miRNA-155. The Ti_3C_2/FePcQDs-based aptasensor displays superior sensing property for the miRNA-155 detection without the use of labeled probe or any electrochemical indicators, giving the detection limit of 4.3 aM within the miRNA-155 concentration ranging from 0.01 fM to 10 pM. The conductance change could also be used for the design of electrochemical sensor.

Zhang, J. L. et al. [68] constructed an conductometric electrochemical sensor by using the Ti_3C_2 MXene as the signal amplified transduction material for the Mycobacterium tuberculosis (M. tuberculosis) detection. After the hybridization between the capture probe peptide nucleic acid (PNA) and the specific fragment of 16S rDNA on the substrate of PNA-AuNPs nanogap network electrode, the target fragments were directly linked with conductive Ti_3C_2 MXene by strong interactions between zirconium-cross-linked Ti_3C_2 MXene and phosphate groups of the target fragments. The linking of Ti_3C_2 MXene to the hybridized target fragments would bridge the gaps of the interrupted AuNPs in the nanogap network electrode and forming the conductive connection to cause the change in conductance between the electrodes. The LOD of proposed method was 20 CFU/mL.

Besides, Wang, H. Y. et al. [69] fabricated a competitive cDNA–Fc/MXene/Apt/Au/GCE aptasensor based on a cDNA–Fc/MXene probe to detect the breast cancer marker Mucin1 (MUC1). When the detection was con-

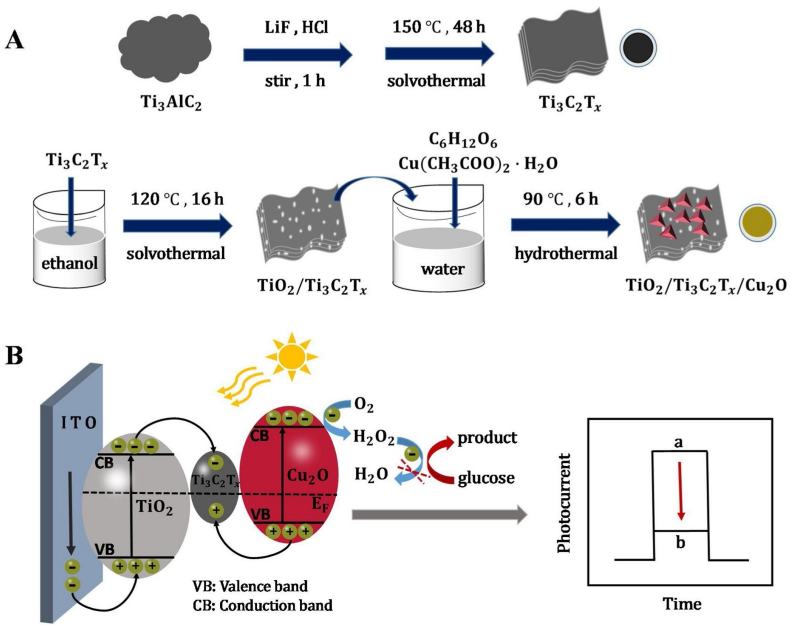

Fig. 15. (A) Preparation process of $Ti_3C_2T_x$ MXenes, $TiO_2/Ti_3C_2T_x$ nanosheets, and $TiO_2/Ti_3C_2T_x/Cu_2O$ composites. (B) Charge transfer and glucose sensing mechanism over the $TiO_2/Ti_3C_2T_x/Cu_2O$ PEC system under visible light irradiation. (Reprinted from [24a] with permission: © 2020 Elsevier B.V.)

Fig. 16. The photograph of fabricated MXene paper with excellent flexibility. (Reprinted from [98] with permission: © 2019 Elsevier B.V.)

ducted, a competitive process happens between the cDNA–Fc/MXene probe and MUC1, which makes cDNA–Fc/MXene probe detach from the sensing electrode, resulting in a decrease in electrical signal. The proposed competitive electrochemical aptasensor gave a wide linear range of 1.0 pM-10 mM and a LOD of 0.33 pM.

There were also some other aptasensors based on MXene, such as MoS_2@$Ti_3C_2T_x$ MXene hybrid-based one for sensitive and rapid quantification of thyroxine (T4) [71], AuNPs/Ti_3C_2 MXene three-dimensional nanocomposite based one for for sensitive miRNA-155 detection [67], and Prussian Blue (PB)/Ti_3C_2 hybrid based one for exosomes detection [70]. They are all listed in the Table 2.

3.2 Electrochemical Non-biosensors

MXene could also be applied in the fabrication of electrochemical non-biosensors without immobilizing enzymes. The first electrochemical non-biosensor based on pristine Ti_3C_2 MXene was fabricated in 2018 for the detection of drinking water contaminant BrO_3^- [38] in which the Ti_3C_2 MXene acting as signal enhancing matrix and reducing agent showed unique electrocatalytic properties towards effective BrO_3^- reduction. After that, two Ti_3C_2 MXene modified GCE electrochemical sensors similar with the first one were fabricated for the detection of pesticide carbendazim [111] and neurotransmitter dopamine [112]. In the former, the redox of carbendazim with lower overpotentials was achieved compared to the graphene-based sensor [113]. The latter achieved a robust sensitivity with a LOD of ~3 nM for dopamine detection in real samples.

Introducing the MXenes into other electrode system like graphite composite paste electrode (GCPE) [51] and screen-printed electrode (SPE) [114] were also be tried. The MXene/GCPE electrochemical sensor was fabricated for the detection of adrenaline. And it is the first time to introduce Ti_2C MXene into the electrochemical sensing system. The prepared sensor achieved a LOD of 9.5 nM and could be further employed in the detection of adrenaline in pharmaceutical samples with 99.2–100.8 % recoveries. The MXene/SPE electrochemical sensor was developed for the simultaneous voltammetric determination of acetaminophen (ACOP) and isoniazid (INZ). The Ti_3C_2 MXene showed excellent electrocatalytic activity toward the oxidation of ACOP and INZ compared with bare SPE in 0.1M H_2SO_4, and the separated oxidation peak potentials ensured simultaneous detection of the targets. The prepared sensor achieved LODs of 0.048μM and 0.064mM for ACOP and INZ respectively.

Besides, the Ti_3C_2 MXene were also integrated into various composites or hybrids with other materials or molecules for different specific analytical purposes, such

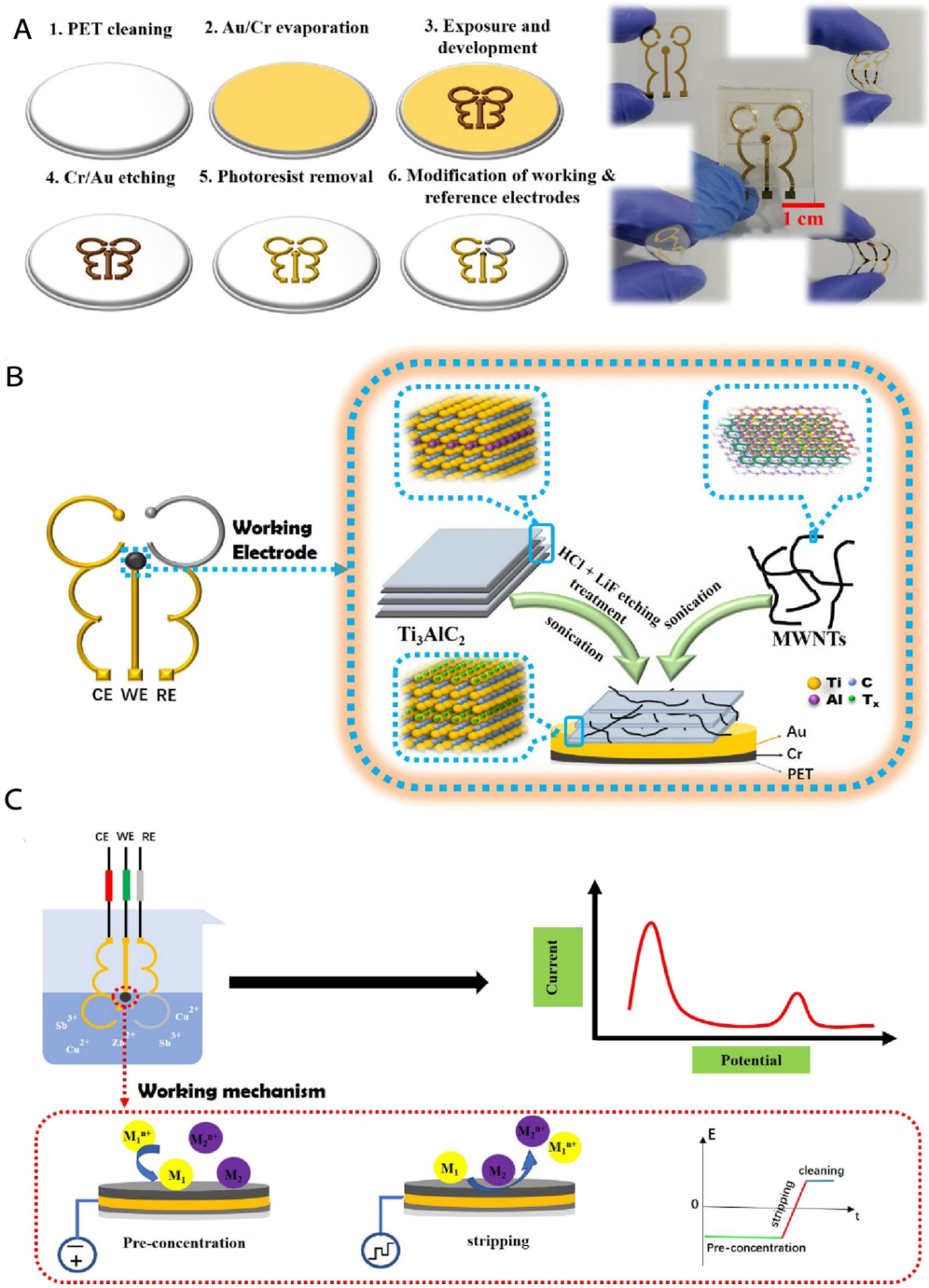

Fig. 17. (A) Fabrication sequences of the proposed flexible $Ti_3C_2T_x$/MWNTs/Au/PET electrode. (B) Modification process of the working electrode. (C) Working mechanism for heavy metal detection. (Reprinted from [24b] with permission: © 2020 American Chemical Society)

as NiO/Ti_3C_2 hybrid for non-enzymatic H_2O_2 sensing [32], three-dimensional porous Ti_3C_2/NiCo-LDH nanocomposite (Nickel-Cobalt layered double hydroxide) for non-enzymatic glucose sensing [34], Au NPs/Ti_3C_2 composite for the sensitive detection of nitrite [115], Pd@Ti_3C_2 nanocomposite for the rapid and real-time detection of l-cysteine (l-Cys) [53], $Mn_3(PO_4)_2$/Ti_3C_2 composite synthesized using adenosine triphosphate (ATP) as a template for amperometric detection of superoxide anions $O_2^{\bullet-}$ from HepG2 cells [39], self-assembled Ti_3C_2/MWCNTs (multi-walled carbon nanotubes) nanocomposite for electrochemical simultaneous detection of hydroquinone (HQ) and catechol (CT) [54], as well as methylene blue (MB)/Cu NPs/Ti_3C_2 composite ratiometric electrochemical detection of piroxicam [116]. In these works, the Ti_3C_2

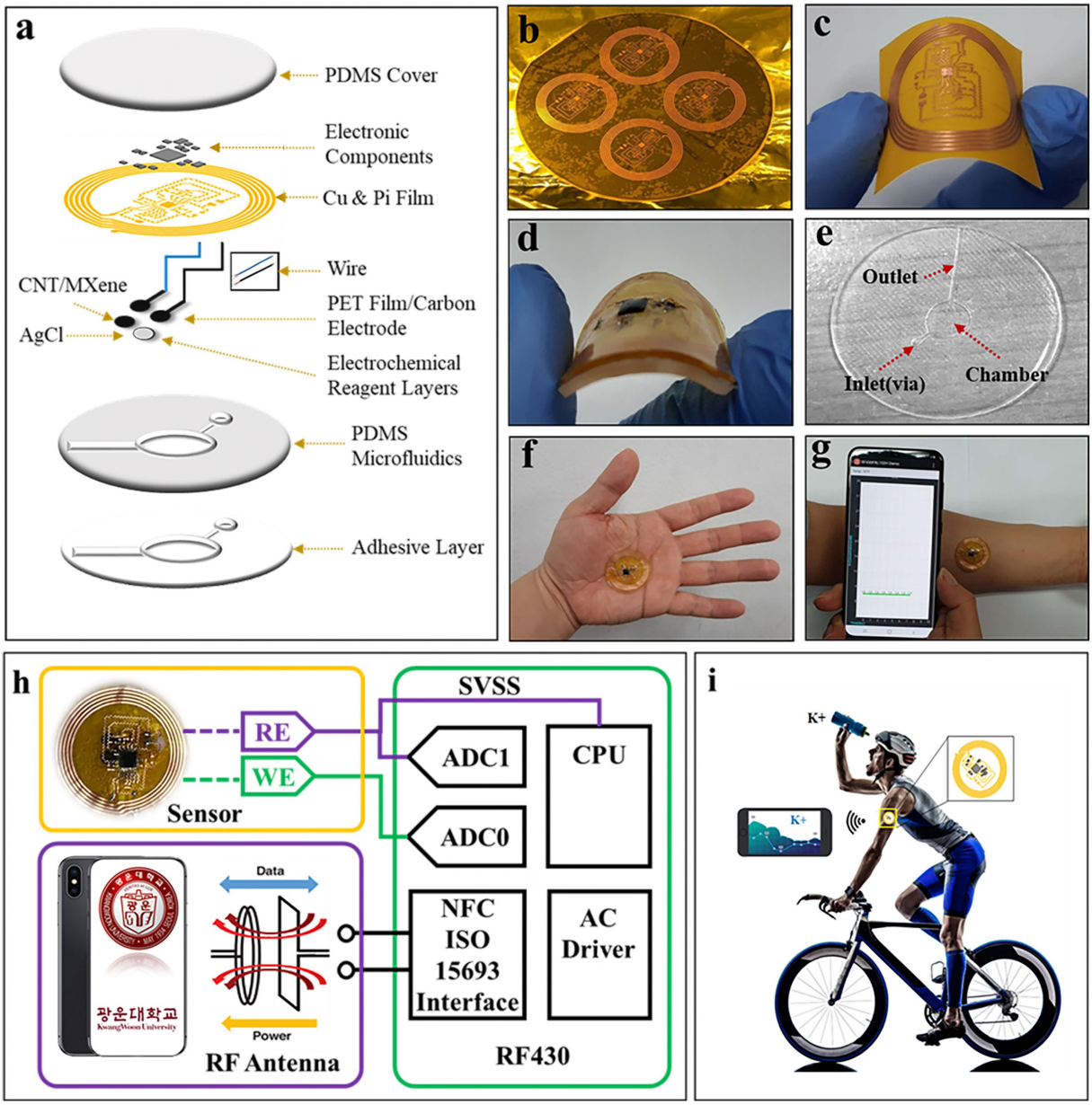

Fig. 18. a) Schematic illustrating the exploded view of the wireless, battery-free, flexible, microfluidic/electronic system. b, c) The lithography and etching process is used to make the flexible antenna and circuits. d) Encapsulation of flexible circuits with PDMS. e) The microfluidic system. f) A very light and small size (diameter: 3.3 cm) circular patch sensor system. g) Wireless NFC sensor and smartphone communication in real-time. h) Electronics design, measurement strategy, and complete system. i) Measuring the electrolyte losses from athletes' sweat could help health professionals plan personalized water and electrolyte replacement strategies. (Reprinted from [100] with permission: © 2020 Elsevier B.V.)

MXene all showed great performance for the fabrication and operation of electrochemical sensors.

MXene is inclined to restack due to the hydrogen bonding and van der Waals interactions between the MXene sheets, which could cause a sharp decrease in the active surface area, further restraining its electrochemical performance [72–73]. To compensate for this shortcoming, Tu, X. L. et al. [72] introduced carbon nanohorns (CNHs) to acted as the spacer and synthesized Ti_3C_2/CNHs nanocomposites (Figure 8). The layered structural MXene/CNHs offered high conductivity, superior catalytic activity and more channels for diffusion of ions. Based on the nanocomposites, they fabricated a carbendazim electrochemical sensor with low limit of detection of 1.0 nM. Besides, Huang, R. M. et al. [73] introduced MOF-5-NH_2-derived nitrogen-doped porous carbon (N-PC) as the spacer to prevent Ti_3C_2 MXene sheets from restacking and fabricated an alk-Ti_3C_2/N-PC electrochemical sensor to detect hydroquinone (HQ) and catechol (CT) in industrial wastewater (Figure 9). Apart from the

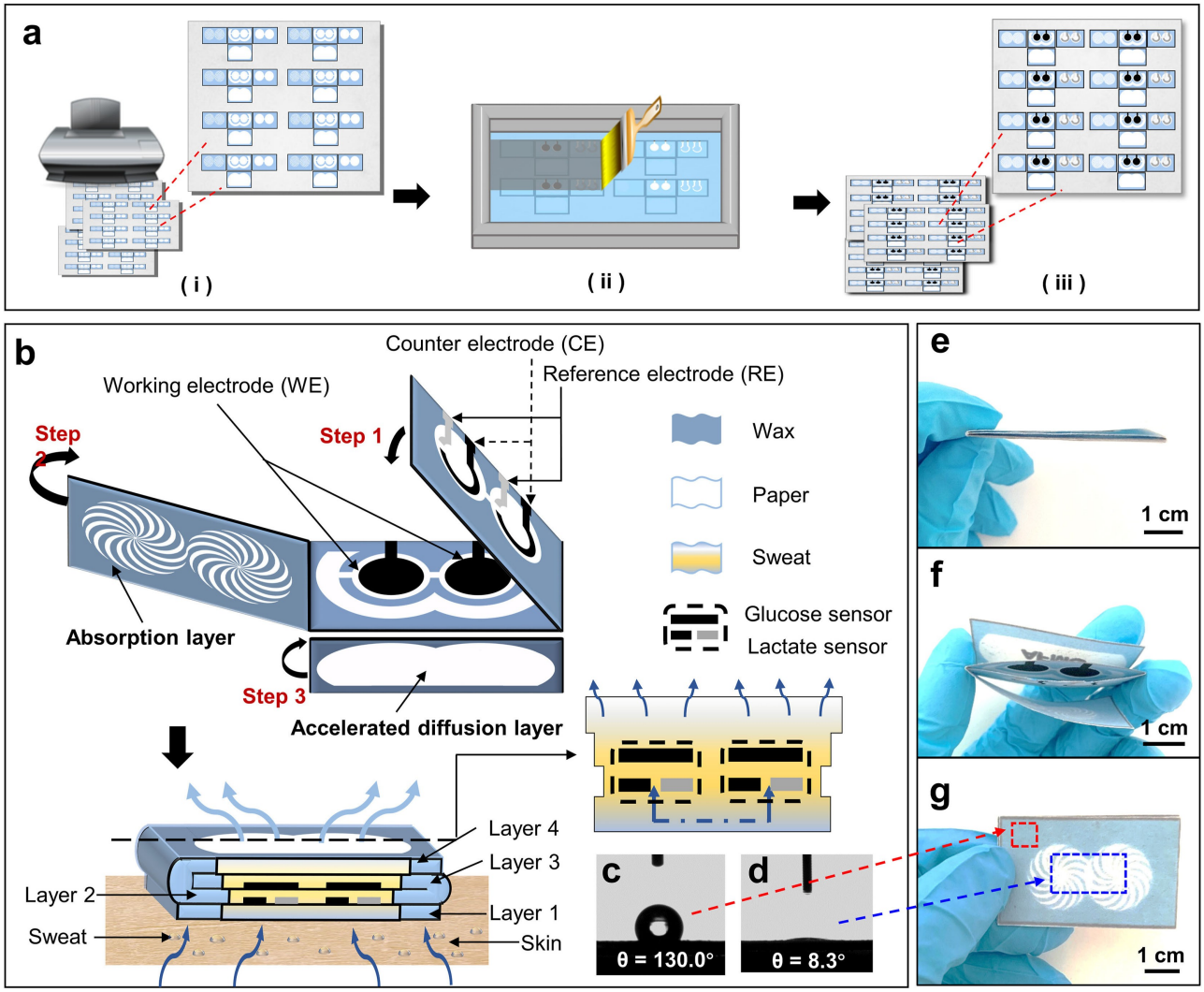

Fig. 19. Schematic illustration and photos of the HIS paper. (a) Schematic illustration of the fabrication of HIS paper. (b) Structural anatomy of HIS paper. (c, d) Contact angle tests on hydrophobic and hydrophilic regions of the HIS paper. (e, g) Photographs of the foldable HIS paper. (Reprinted from [102] with permission: © 2020 Elsevier B.V.)

combination of N-PC for the restacking of Ti_3C_2, they gave an alkaline intercalation treatment to the Ti_3C_2 MXene sheets because the surface of alkalization-intercalated MXene may offer abundant –OH groups, which were more likely to sense HQ and CT based on hydrogen-bond interaction. The alk-Ti_3C_2/N-PC electrochemical sensor for the detection of hazardous HQ and CT showed LODs of 4.8 nM and 3.1 nM for HQ and CT respectively with a wide linear range from 0.5 μM to 150 μM.

Selectivity is a bottleneck that plagues the application of electrochemical sensors in tracking measurements and molecularly imprinted polymers can be viewed as a modified material that enhances selectivity of sensors with specific recognition property, low cost and short synthesis time [75]. Ma, X. et al. [75] developed a selective and sensitive electrochemical sensor for fisetin detection based on hierarchical porous Ti_3C_2 MXene/amino carbon nanotubes (MXene/NH_2-CNTs) composite and MIP (Figure 10). The Ti_3C_2 MXene/NH_2-CNTs composite was prepared by self-assembly of negatively charged Ti_3C_2 flakes and positively charged NH_2-CNTs. The amino functionalized CNTs not only owned good conductivity, but also had positive electricity on their surface which could act as interlayer spacers to avoid the aggregation of Ti_3C_2 MXene. The fabricated MIP/Ti_3C_2 MXene/NH_2-CNTs/GCE showed a high analytical performance for fisetin determination with a LOD of 1.0 nM.

There are also many other advances in the MXene-based electrochemical non-biosensors. For the real-time and in-situ detection of H_2O_2 secreted from living cells, Dang, Y. et al. [74] fabricated a electrochemical biosensor based on PB NPs intercalated Ti_3C_2 nanosheets (PB NPs/Ti_3C_2) obtaining a low limit of detection (0.20 μM) to H_2O_2. And besides the prepared PB/Ti_3C_2 showed negligible cytotoxicity to normal fibroblast cells at all tested time points and concentrations, validating its potential

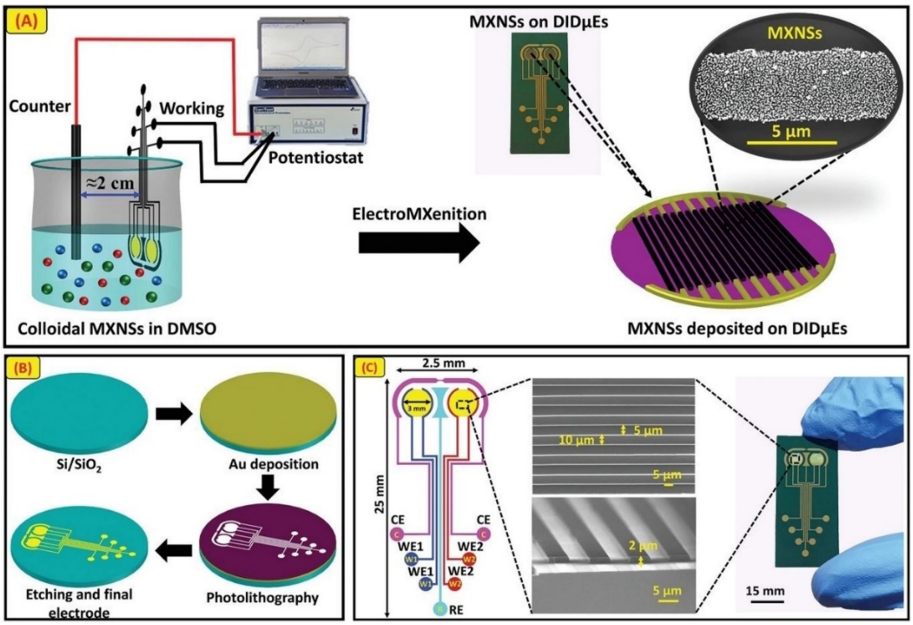

Fig. 20. A) Schematic illustration of the customized electrolyte bath and the electroMXenition process. B) Standard single-masked UV photolithography and etching procedures to fabricate DIDμE. C) Mapping of the sensor, an optical image of the real sensor, and FESEM images of the top and cross-sectional views of the interdigitated patterns. (Reprinted from [97] with permission: © 2020 Wiley-VCH GmbH)

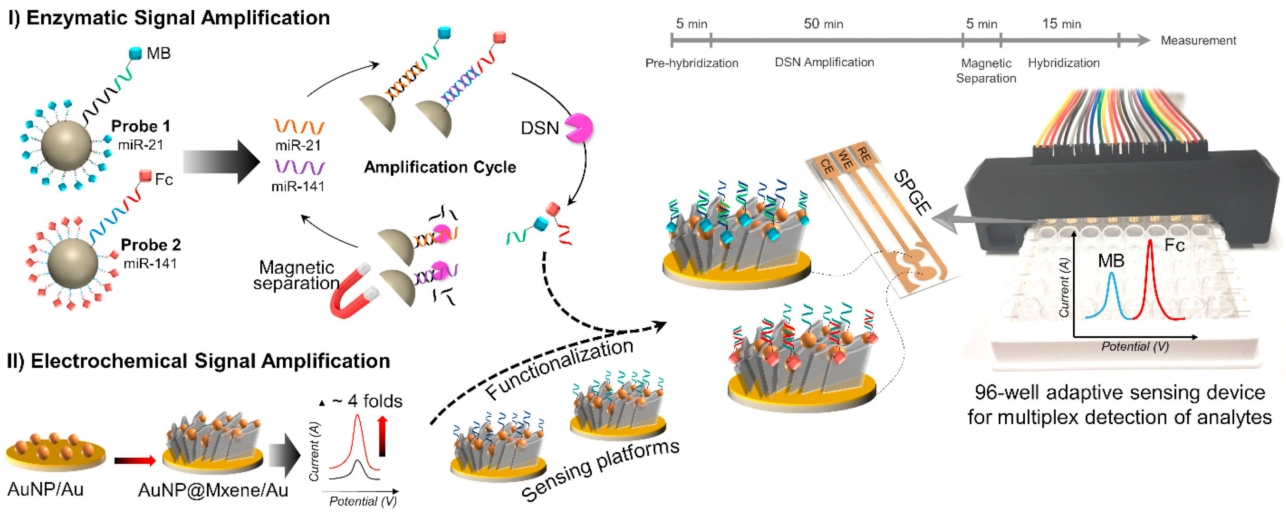

Fig. 21. Schematic diagram representing the whole assay procedure for multiplex and concurrent detection of miR-21 and miR-141. (Reprinted from [101] with permission: © 2020 Elsevier B.V.)

application in living cell concerned fields. For the detection of sulfadiazine, Kokulnathan, T. et al. [77] synthesized Ti_3C_2/BN nanocomposites and fabricated a Ti_3C_2/BN-modified electrode as the electrochemical catalytical sensor showing a trace-level limit of detection (3.0 nM). Kalambate, P. K. et al. [78] developed an electrochemical sensor for the detection of ifosfamide (IFO), acetaminophen (ACOP), domperidone (DOM), and sumatriptan (SUM) based on self-assembled MXene/MWCNT/Chitosan nanocomposite thin film and got LODs for IFO, ACOP, DOM, and SUM of 0.00031, 0.00028, 0.00034, and 0.00042 μM, respectively. Other various analytes like uric acid (UA) and folic acid (FA) [79], NO_2^- [80–81], 4-nitroquinoline N-oxide (4-NO) [85], Pb^{2+} and Cd^{2+} heavy metal ions [82–84], hydrazine [86] and dopamine [87] are all listed in the Table 2. The Nb-based MXene [117] and V-based MXene [76] for electrochemical sensing have also been concerned.

3.3 Electrochemiluminescence Sensors

The first ECL sensors based on the Ti_3C_2 MXene was constructed in 2018 [118] by Fang, Y. F. et al. The Ti_3C_2 MXene has a negatively charged surface due to the existence of –F and –OH/=O surface groups, which make it much favorable for $Ru(bpy)_3^{2+}$ immobilization via electrostatic attraction. And the utilization of Ti_3C_2 MXene not only allowed the composite film to have much higher conductivity, but also enhance the adsorption amount of $Ru(bpy)_3^{2+}$. The as-proposed Ru/MXene sensor showed a stable and excellent ECL performance and was used for the label-free single-nucleotide mismatch discrimination in human urine. After that, a sensitive ECL biosensor was developed for the detection of exosomes using aptamer modified Ti_3C_2 MXene as the ECL nanoprobe [119]. The prepared ECL biosensor obtained a LOD of 125 particles/mL, which was over 100 times lower than that of conventional enzyme-linked immunosorbent assay (ELISA) method.

Huang, W. et al. [91] utilized the Ti_3C_2 MXene nanosheets as carriers to graft $Ru(bpy)_2(mcpbpy)^{2+}$ (bpy = 2,2′-bipyridine, mcpbpy = 4-(4′-methyl-[2,2′-bipyridin]-4-yl) butanoic acid) obtaining 2D ultrathin Ru-complex-grafted MXene nanosheets (Ru@MXene). In their work, $Ru(bpy)_2(mcpbpy)^{2+}$ acted as both an ECL luminophore and an intercalation molecule achieving surface functionalization and delamination of multilayered Ti_3C_2. They used the Ru@MXene to construct an ECL sensor for the determination of MUC1, which displayed a low LOD of 26.9 ag/mL.

Just like other electroanalysis methods, false errors may occur in electrochemiluminescence sensing resulting from some external environmental changes, such as the coreactant concentration, temperature, pH, etc, and in order to overcome these limitations, many ECL ratiometric assays have been proposed For the detection of the clinical biomarker carcinoembryonic antigen (CEA), Shang, L. et al. [88] developed a sandwich dual-potential ratiometric ECL sensor using luminol as single luminophore based on graphene-ionic liquid-platinum (GR-IL-Pt) composites as matrix to immobilize the Ab_1 and Ti_3C_2/AuNPs hybrids as platform to load the Ab_2 (Figure 11). During the cyclic potential scanning, luminol exhibited $ECL_{cathodic}$ and ECL_{anodic} on GR-IL-Pt composites and Ti_3C_2/AuNPs hybrids at different potentials, respectively (Figure 12). And the ratio of anodic ECL to cathodic ECL ($ECL_{anodic}/ECL_{cathodic}$) increased with the concentration of CEA, realizing sensitive ratiometric detection of CEA. The developed ECL sensor exhibited a sensitive detection toward CEA, with a low LOD of 34.58 fg/mL.

MXene also has excellent superior photothermal conversion efficiency, and this property has been utilized by researchers to develop a photothermal amplification strategy for ECL sensors [89]. Fang, D. et al. [28] constructed an ECL and photothermal dual-mode biosensor for the determination of exosomes by utilizing a Ti_3C_2 MXene-black phosphorous quantum dots (BPQDs) probe (Figure 13). The Ti_3C_2 MXene was utilized as supporter to immobilize BPQDs and $Ru(dcbpy)_3^{2+}$. The Ti_3C_2 MXene and BPQDs both possessed extraordinary photothermal properties, and were utilized to construct the ECL and temperature dual-mode sensor. For ECL detection, the sensor showed a LOD of 37.0 particles/μL, while for photothermal detection, the temperature increase (ΔT) was linearly correlated with the logarithm of exosomes concentration in the range from 1.1×10^2 to 1.1×10^7 particles/μL. They also [89] constructed a photothermal amplified cathodic ECL immunosensor based on a probe of Nb_2C MXene immobilized ZnO quantum dots (QDs) for thyroglobulin detection (Figure 14). Nb_2C MXene was employed as scaffold to load ZnO QDs, $Ru(bpy)_3^{2+}$ and Ab_2, and acted as temperature controller to increase the electrode surface temperature by converting laser energy into heat. The ECL intensity strengthened gradually with Tg concentration increased in the range from 1 fg/mL to 10 ng/mL at the electrode surface temperature at 40 °C, but in a narrower range (0.1 pg/mL to 1 ng/mL) when the electrode surface temperature was changed to 25 °C. This result successfully demonstrated the photothermal amplified strategy could improve the ECL sensor's sensitivity.

3.4 Photoelectrochemical Sensors

The first MXene-based PEC sensor was based on a Ti_3C_2 MXene/Cu_2O heterostructure for the detection of glucose [35]. The Ti_3C_2 MXene/Cu_2O composite showed excellent PEC performance and sensitive photoelectric response to glucose with a LOD of 0.17 nM. After that, a TiO_2 inverse opal photonic crystals (IOPCs)/Ti_3C_2 quantum dots (QDs) composite film was prepared for the detection of glutathione [120]. The TiO_2 IOPCs/Ti_3C_2 composite film could have photocurrent effect from 280 to 900 nm, and the internal power conversion efficiency could reach to 26 % at 350 nm. These results both show the great potential of Ti_3C_2 MXene in the PEC sensors.

A controlled oxidation of MXene is able to create transition metal oxide particles on sheets of MXene and is an efficient way to alter the surface properties of MXene [93]. Soomro, R. A. et al. [92] constructed a photoactive heterojunction comprising of in-situ grown TiO_2 from few-layer thin Ti_3C_2 nanosheets in conjunction with visible-light active lysine functionalized $BiVO_4$ nanoparticles. The obtained $TiO_2/Ti_3C_2/BiVO_4$ heterojunction, based on its in-situ hybrid configuration, exhibited an ideal interfacial arrangement capable of supporting high photocatalytic redox-activity with minimum interfacial recombination. They fabricated a PEC biosensor with this heterojunction to detect soluble CD44 protein realizing an extremely low LOD of 0.000014 ng/mL.

Han, F. et al. [93] developed a one-step process of TiO_2 particles grown on MXene sheets by hydrogen peroxide (H_2O_2) oxidation of Ti_3C_2 under heat treatment to fabricate Ti_3C_2-TiO_2 composites. Based on the Ti_3C_2–TiO_2 composites they established a PEC sensor to

evaluate ascorbic acid (AA) and its interaction with other antioxidants including gallic acid (GA), vitamin E (VE), epigallocatechin (EGC), epigallocatechin gallate (EGCG) and proanthocyanins (PC). They found that there was obvious antioxidant synergism between AA and other antioxidants, because AA with the low redox potential could reduce other antioxidants radical to promote regeneration, improving the overall antioxidant performance. As a result, they successfully applied the prepared PEC sensor to determine the antioxidant capacity of health product of grape seed and vitamin C&E.

For glucose detection, Chen, G. et al. [24a] fabricated a Z-scheme $TiO_2/Ti_3C_2/Cu_2O$ heterostructure and employed it as a photocathode to construct a self-powered PEC sensor (Figure 15). The artificial indirect "Z-scheme" system was exploited through binding two semiconductors (two separated photosystems (PS)) with electron mediators. In their work, the TiO_2 NPs were in situ generated on the Ti_3C_2 nanosheets by ethanol thermal treatment of the Ti_3C_2 MXene and the Z-scheme $TiO_2/Ti_3C_2/Cu_2O$ heterojunction was prepared by hybridizing with the narrow bandgap semiconductor Cu_2O. The Z-scheme $TiO_2/Ti_3C_2/Cu_2O$ heterojunction exhibited superior PEC performance than TiO_2/Ti_3C_2 and Cu_2O and based on which the $TiO_2/Ti_3C_2/Cu_2O$ PEC sensor for glucose showed a remarkable low LOD of 33.75 nM with a wide range of 100 nM to 10 μM.

Besides, Soomro, R. A. et al. [94] constructed an in-situ engineered heterojunction using partially-oxidized Ti_3C_2 sheets and photo-active $NiWO_4$ nanoparticles. The designed $TiO_2/Ti_3C_2/NiWO_4$ PEC platform was applied for the detection of PSA with a LOD down to 0.15 fg/mL. Yuan, C. et al. [95] proposed a $g\text{-}C_3N_4/Ti_3C_2$ composite as a photoelectrochemical sensing material for the detection of ciprofloxacin (CFX) and the PEC sensor showed a LOD of 0.13 nM with a dynamic range from 0.4 to 1000 nM. Jiang, Q. Q. et al. [96] constructed a PEC sensor for Hg^{2+} detection on the heterojunction between Ti_3C_2 MXene and $BiVO_4$ semiconductor through simply spin-coating the single-layer Ti_3C_2 onto the surface of $BiVO_4$ film. The PEC sensor displayed a wide linear range from 1 pM to 2 nM with the limit of detection down to 1 pM and also exhibited satisfactory accuracy and repeatability in practical sample water, the Yangtze River water.

3.5 Flexible Electrochemical Sensors and Others

Flexibility plays crucial roles in the application of paper substrate for constructing advanced implantable biomedical devices and miniaturized lap-on-a-chip devices when applying in the assay of real samples [98]. Different from traditional rigid sensing platforms, flexible sensing platforms could facilely form good interface with the curvature of soft biological materials such as cells or human skin, which can promote significantly improved detection performance of biological signal molecules, such as the pressure-based electrochemical flexible sensors [99,121]. Flexible sensors are seriously affected by interface materials. The introduction of MXene has been proved to be effective way.

Yao, Y. et al. [98] fabricated a kind of flexible biomimetic Ti_3C_2 MXene paper with noble metal nanoparticles (Figure 16). The obtained hybrid Ti_3C_2 MXene papers, showing outperforming electrocatalytic activities, satisfactory biocompatibility, excellent stability and flexibility, were able to serve as high-performance extracellular biosensing platforms for the sensitive monitoring of superoxide ($O_2^{\bullet-}$) secreted by living cells. The amperometric response to 0.5 μM $O_2^{\bullet-}$ at the widest bending angle (90°) after 50 continuous bending times could keep 80.1 % of that at original state indicating that the Ti_3C_2 MXene paper exhibited satisfactory performance towards bending-induced mechanical stress. Zhao, S. F. et al. [99] fabricated a $Ti_3C_2/Mn_3(PO_4)_2$ based flexible electrochemical sensor for real-time and quantitatively monitoring $O_2^{\bullet-}$ released from human lung cancer cells. They designed a $Mn_3(PO_4)_2$ based biomimetic enzyme by interracially assembling 2-D $Mn_3(PO_4)_2$ and Ti_3C_2 MXene nanosheets into a 2-D/2-D heterostructure. The 2-D nature of the two components with strong interfacial interaction synergistically enabled the heterostructure an excellent flexibility with retained 100 % of the response when to reach a bending angle up to 180°, and 96 % of the response after 100 bending/relaxing cycles. The fabricated sensor achieved a low LOD of 1.63 nM.

Besides, Hui, X. et al. [24b] fabricated a flexible electrochemical sensor based on a gold electrode modified with Ti_3C_2 MXene and multiwalled carbon nanotubes (MWCNTs) for the detection of copper (Cu) and zinc (Zn) ions (Figure 17). The MWCNTs were incorporated as the anti-pile layers and spacers to mitigate the aggregation problem between the Ti_3C_2 layers and to expose more surface area and active sites of Ti_3C_2 layers. Compared with the stripping current measured in the normal state, the peak current changed by approximately 1.3, 0.6, and 1.9 % at the bending degrees of 70, 45, and 30°, respectively, and even after several times (n = 55) of bending. Owing to its small size and portability, their proposed Ti_3C_2/MWCNTs-modified Au/PET sensor could achieve on-site heavy metal analysis and could be applied to homecare smart heavy metal monitoring systems or other clinical medicine studies.

There were also some attentions being focused on wearable biosensors for measuring biomarkers in body fluids like sweat, tears and saliva to reflect the physiological state of the body [100]. Zhang, S. et al. [100] developed an ultra-high sensitive, flexible, wireless, battery-free, and fully integrated (no external analysis equipment) electrochemical sensing patch system, including a microfluidic-sweat collecting unit, for the on-site monitoring of the K^+ concentration in human sweat (Figure 18). And in order to on-site detect potassium concentration in human sweat, the flexible electrochemical sensor was integrated and assembled with a low-power radio frequency (RF) energy harvesting battery-free near field communication (NFC) wireless patch

system to wirelessly transmit measurements to a smartphone. The smartphone was used as an RF power source to wirelessly activate NFC electronic systems and receive sensing data from the device. An application developed based on an android studio software program was used to display the detection K^+ concentration values. At the same time, a microfluidic channel was integrated with the electrochemical sensor patch to efficiently collect sweat on human skin surface and mitigate the sensor surface contamination problem. The fabricated sensor measured the K^+ concentration of human sweat with a high sensitivity 173 mV/dec with a high linear range from 1 to 32 mM. Li, M. et al. [102] designed a highly integrated sensing (HIS) paper by employing Ti_3C_2 as the active materials and foldable all-paper substrates as sweat analysis patch, which integrated a signal processing system that was able to simultaneously detect lactate and glucose for real-time analysis of sweat (Figure 19). The different functional areas of HIS paper were printed on paper substrate, followed by folding it into three-dimensional structure and attributed to the well-designed 3D diffusion path as well as hydrophilic effect of paper substrates. Human sweat could be efficiently collected and rapidly diffuse along vertical direction from the human-device interfaces. A dual-channel electrochemical sensor that could simultaneously detect glucose and lactate with sensitivity of 2.4 nA/μM and 0.49 μA/mM respectively was produced based on the HIS paper by them. The low cost and convenient HIS paper has the potential for practical application of non-invasive electrochemical sensors and wearable bioelectronic products.

In the fabrication of various electrochemical sensing devices, arranging nanomaterials into a particular position on a patterned electrode with controlled architecture, morphology, and thickness is a most challenging issue [97]. For obtaining large-scale and high-quality MXene nanosheets thin films, Sharifuzzaman, M. et al. [97] reported a green, facile, and cost-effective one-pot deposition mechanism of Ti_3C_2 nanosheets (Figure 20). They demonstrated that Ti_3C_2 nanosheets can be precisely and uniformly deposited on different sensing electrodes at room temperature within a few minutes via electroplating technique using a DMSO suspension with colloidal Ti_3C_2 nanosheets as an electrolyte. Ti_3C_2 nanosheets disperse completely and were highly stable in DMSO solvent. The redox reaction in the colloidal Ti_3C_2 nanosheets solution under the effect of a constant applied potential generated an electric field, which drives the nanoparticles toward a specific electrode interface so that they were catholically electroplated. By this method, they fabricated a miniaturized Ti_3C_2-AFBPB-film-modified dual interdigitated microelectrode (DIDμE) label-free immunosensor for the simultaneous and multiplexed detection of bladder cancer biomarkers detection (Apo-A1 and NMP 22) with the help of a task-specific ionic liquid (TSIL), 4-amino-1-(4-formyl-benzyl) pyridinium bromide (AFBPB). The developed dual immunosensor demonstrated lower LODs (0.3 pg/mL and 0.7 pg/mL, respectively).

Besides, for the specific, sensitive and rapid detection of multiple miRNAs in total plasma, Mohammadniaei, M. et al. [101] casted Ti_3C_2 MXene which modified with 5 nm gold nanoparticles (AuNPs) on a dual screen-printed gold electrode to host vast numbers of DNA probes as a multiplex biosensor for miR-21 and miR-141 (Figure 21). The biosensor showed substantial LOD of 204 aM and 138 aM for miR-21 and miR-141 respectively. And they fabricated a 96-well adaptive sensing device successfully profiling cancer plasma samples. This device could be upgraded for quantification of more analytes to become a prosperous device for point of care (POC).

4 Conclusions and Prospects

MXene has shown great application potential in electrochemical sensors, and many electrochemical sensors based on MXene have been developed including electrochemical non-biosensors, electrochemical biosensors, electrochemiluminescence sensors and photoelectrochemical sensors. In addition, MXene holds great promise in the conductive substrate preparation for various electrode systems, especially for various patterned electrode. This paves the way for the development of various advanced electrochemical sensing devices such as flexible and wearable sensors for non-invasive body fluid monitoring, and miniaturized detection devices for practicably determination.

For the application of MXene in electrochemical sensors in the future, we think there are several directions that can be further studied. (1) For biosensors, MXene are usually applied as a carrier of biomolecules, and the immobilization of biomolecules onto the surface of MXene are generally realized by the assistance of Au nanoparticles or by electrostatic adsorption, we think the direct chemical coupling between biomolecules and MXene is more valuable considering the stability of biocomposites and the abundant surface chemistry of MXene. It means that the functionalization of the surface of MXene like amination or carboxylation is an important subject. Noteworthily, the electrochemical etching (E-etching) exfoliation route is very interesting [62]. The simultaneous realization of chemical group functionalization and exfoliation of MXene by electrochemical route is very attracting. (2) The good photothermal conversion efficiency of MXene open the door of the application of new sensitivity enhancement strategy. We think this strategy is very promising and could be adopted in other type electrochemical sensors in addition to ECL sensors [28,89]. (3) For photoelectrochemical sensors and flexible sensors, the structure of heterojunctions and composition of conductive and sensing film are decisive. More combinations could be explored. In a word, with MXene as a powerful right hand, more advanced electrochemical sensors can be expected in the future.

Acknowledgements

This work was supported by the National Natural Science Foundation of China (Grant Nos. 22074052 and 22004046).

Data Availability Statement

Data sharing is not applicable to this article as no new data were created or analyzed in this study.

References

[1] K. H. Lubert, K. Kalcher, *Electroanalysis* **2010**, *22*, 1937–1946.
[2] J. M. Diaz-Cruz, N. Serrano, C. Perez-Rafols, C. Arino, M. Esteban, *J. Solid State Electrochem.* **2020**, *24*, 2653–2661.
[3] N. J. Ronkainen, H. B. Halsall, W. R. Heineman, *Chem. Soc. Rev.* **2010**, *39*, 1747–1763.
[4] a) W. Miao, *Chem. Rev.* **2008**, *108*, 2506–2553; b) L. Hu, G. Xu, *Chem. Soc. Rev.* **2010**, *39*, 3275–3304; c) K. Muzyka, *Biosens. Bioelectron.* **2014**, *54*, 393–407; d) W.-W. Zhao, J.-J. Xu, H.-Y. Chen, *Chem. Rev.* **2014**, *114*, 7421–7441; e) A. Devadoss, P. Sudhagar, C. Terashima, K. Nakata, A. Fujishima, *Journal of Photochemistry and Photobiology C-Photochemistry Reviews* **2015**, *24*, 43–63; f) Z. Liu, W. Qi, G. Xu, *Chem. Soc. Rev.* **2015**, *44*, 3117–3142; g) W.-W. Zhao, J.-J. Xu, H.-Y. Chen, *Chem. Soc. Rev.* **2015**, *44*, 729–741; h) W.-W. Zhao, J.-J. Xu, H.-Y. Chen, *Anal. Chem.* **2018**, *90*, 615–627.
[5] J. Shu, D. Tang, *Anal. Chem.* **2020**, *92*, 363–377.
[6] Q. Zhou, D. Tang, *TrAC Trends Anal. Chem.* **2020**, *124*, 115814.
[7] a) C. Chen, M. La, *Int. J. Electrochem. Sci.* **2020**, *15*, 6852–6862; b) M. La, *Int. J. Electrochem. Sci.* **2020**, *15*, 6436–6447; c) D. Liu, M. La, *Int. J. Electrochem. Sci.* **2020**, *15*, 11371–11386; d) W. Tu, Z. Wang, Z. Dai, *TrAC Trends Anal. Chem.* **2018**, *105*, 470–483; e) Z. Wang, R. Yu, H. Zeng, X. Wang, S. Luo, W. Li, X. Luo, T. Yang, *Microchim. Acta* **2019**, *186*, 405; f) Y. Zhou, H. Yin, W.-W. Zhao, S. Ai, *Coord. Chem. Rev.* **2020**, *424*, 213519.
[8] C. Z. Zhu, G. H. Yang, H. Li, D. Du, Y. H. Lin, *Anal. Chem.* **2015**, *87*, 230–249.
[9] P. K. Kannan, D. J. Late, H. Morgan, C. S. Rout, *Nanoscale* **2015**, *7*, 13293–13312.
[10] B. Anasori, M. R. Lukatskaya, Y. Gogotsi, *Nat. Rev. Mater.* **2017**, *2*, 16098.
[11] K. S. Novoselov, A. K. Geim, S. V. Morozov, D. Jiang, Y. Zhang, S. V. Dubonos, I. V. Grigorieva, A. A. Firsov, *Science* **2004**, *306*, 666–669.
[12] G. R. Bhimanapati, Z. Lin, V. Meunier, Y. Jung, J. Cha, S. Das, D. Xiao, Y. Son, M. S. Strano, V. R. Cooper, L. B. Liang, S. G. Louie, E. Ringe, W. Zhou, S. S. Kim, R. R. Naik, B. G. Sumpter, H. Terrones, F. N. Xia, Y. L. Wang, J. Zhu, D. Akinwande, N. Alem, J. A. Schuller, R. E. Schaak, M. Terrones, J. A. Robinson, *ACS Nano* **2015**, *9*, 11509–11539.
[13] a) M. Naguib, O. Mashtalir, J. Carle, V. Presser, J. Lu, L. Hultman, Y. Gogotsi, M. W. Barsoum, *ACS Nano* **2012**, *6*, 1322–1331; b) M. Naguib, V. N. Mochalin, M. W. Barsoum, Y. Gogotsi, *Adv. Mater.* **2014**, *26*, 992–1005; c) B. Anasori, Y. Xie, M. Beidaghi, J. Lu, B. C. Hosler, L. Hultman, P. R. C. Kent, Y. Gogotsi, M. W. Barsoum, *ACS Nano* **2015**, *9*, 9507–9516; d) J.-C. Lei, X. Zhang, Z. Zhou, *Frontiers of Physics* **2015**, *10*, 276–286; e) V. M. H. Ng, H. Huang, K. Zhou, P. S. Lee, W. Que, J. Z. Xu, L. B. Kong, *J. Mater. Chem. A* **2017**, *5*, 3039–3068.
[14] M. Alhabeb, K. Maleski, B. Anasori, P. Lelyukh, L. Clark, S. Sin, Y. Gogotsi, *Chem. Mater.* **2017**, *29*, 7633–7644.
[15] L. Verger, C. Xu, V. Natu, H. M. Cheng, W. C. Ren, M. W. Barsoum, *Curr. Opin. Solid State Mater. Sci.* **2019**, *23*, 149–163.
[16] J. B. Pang, R. G. Mendes, A. Bachmatiuk, L. Zhao, H. Q. Ta, T. Gemming, H. Liu, Z. F. Liu, M. H. Rummeli, *Chem. Soc. Rev.* **2019**, *48*, 72–133.
[17] M. Sajid, *Anal. Chim. Acta* **2021**, *1143*, 267–280.
[18] L. Lu, X. Han, J. Lin, Y. Zhang, M. Qiu, Y. Chen, M. Li, D. Tang, *Analyst* **2021**, *146*, 2664–2669.
[19] R. Zeng, W. Wang, M. Chen, Q. Wan, C. Wang, D. Knopp, D. Tang, *Nano Energy* **2021**, *82*, 105711.
[20] G. Cai, Z. Yu, P. Tong, D. Tang, *Nanoscale* **2019**, *11*, 15659–15667.
[21] D. D. Song, X. Y. Jiang, Y. S. Li, X. Lu, S. R. Luan, Y. Z. Wang, Y. Li, F. M. Gao, *J. Hazard. Mater.* **2019**, *373*, 367–376.
[22] H. Dong, L. Cao, Z. Tan, Q. Liu, J. Zhou, P. Zhao, P. Wang, Y. Li, W. Ma, Y. Dong, *ACS Applied Bio Materials* **2020**, *3*, 377–384.
[23] F. Duan, C. Guo, M. Hu, Y. Song, M. Wang, L. He, Z. Zhang, R. Pettinari, L. Zhou, *Sens. Actuators B* **2020**, *310*, 127844.
[24] a) G. Chen, H. Wang, X. Wei, Y. Wu, W. Gu, L. Hu, D. Xu, C. Zhu, *Sens. Actuators B* **2020**, *312*, 127951; b) X. Hui, M. Sharifuzzaman, S. Sharma, X. Xuan, S. Zhang, S. G. Ko, S. H. Yoon, J. Y. Park, *ACS Appl. Mater. Interfaces* **2020**, *12*, 48928–48937.
[25] Y.-Z. Zhang, Y. Wang, Q. Jiang, J. K. El-Demellawi, H. Kim, H. N. Alshareef, *Adv. Mater.* **2020**, *32*, 1908486.
[26] M. Mathew, S. Radhakrishnan, A. Vaidyanathan, B. Chakraborty, C. S. Rout, *Anal. Bioanal. Chem.* **2021**, *413*, 727–762.
[27] W. Huang, L. Hu, Y. Tang, Z. Xie, H. Zhang, *Adv. Funct. Mater.* **2020**, *30*, 2005223.
[28] D. Fang, D. Zhao, S. Zhang, Y. Huang, H. Dai, Y. Lin, *Sens. Actuators B* **2020**, *305*, 127544.
[29] F. Wang, C. Yang, C. Duan, D. Xiao, Y. Tang, J. Zhu, *J. Electrochem. Soc.* **2015**, *162*, B16-B21.
[30] F. Wang, C. Yang, M. Duan, Y. Tang, J. Zhu, *Biosens. Bioelectron.* **2015**, *74*, 1022–1028.
[31] J. Zheng, J. Diao, Y. Jin, A. Ding, B. Wang, L. Wu, B. Weng, J. Chen, *J. Electrochem. Soc.* **2018**, *165*, B227-B231.
[32] R. Ramachandran, C. Zhao, M. Rajkumar, K. Rajavel, P. Zhu, W. Xuan, Z.-X. Xu, F. Wang, *Electrochim. Acta* **2019**, *322*, 134771.
[33] R. B. Rakhi, P. Nayak, C. Xia, H. N. Alshareef, *Sci. Rep.* **2016**, *6*, 36422.
[34] M. Li, L. Fang, H. Zhou, F. Wu, Y. Lu, H. Luo, Y. Zhang, B. Hu, *Appl. Surf. Sci.* **2019**, *495*, 143554.
[35] M. Li, H. Wang, X. Wang, Q. Lu, H. Li, Y. Zhang, S. Yao, *Biosens. Bioelectron.* **2019**, *142*, 111535.
[36] H. Zou, F. Zhang, H. Wang, J. Xia, L. Gao, Z. Wang, *New J. Chem.* **2019**, *43*, 2464–2470.
[37] H. Liu, C. Duan, C. Yang, W. Shen, F. Wang, Z. Zhu, *Sens. Actuators B* **2015**, *218*, 60–66.
[38] P. A. Rasheed, R. P. Pandey, K. Rasool, K. A. Mahmoud, *Sens. Actuators B* **2018**, *265*, 652–659.
[39] J. Zheng, B. Wang, Y. Jin, B. Weng, J. Chen, *Microchim. Acta* **2019**, *186*, 95.

[40] J. Zheng, B. Wang, A. Ding, B. Weng, J. Chen, *J. Electroanal. Chem.* **2018**, *816*, 189–194.
[41] F. Shahzad, A. Iqbal, S. A. Zaidi, S.-W. Hwang, C. M. Koo, *Journal of Industrial and Engineering Chemistry* **2019**, *79*, 338–344.
[42] L. Zhou, X. Zhang, L. Ma, J. Gao, Y. Jiang, *Biochem. Eng. J.* **2017**, *128*, 243–249.
[43] Y. Jiang, X. Zhang, L. Pei, S. Yue, L. Ma, L. Zhou, Z. Huang, Y. He, J. Gao, *Chem. Eng. J.* **2018**, *339*, 547–556.
[44] D. Song, X. Jiang, Y. Li, X. Lu, S. Luan, Y. Wang, Y. Li, F. Gao, *J. Hazard. Mater.* **2019**, *373*, 367–376.
[45] D. Wu, M. Wu, J. Yang, H. Zhang, K. Xie, C.-T. Lin, A. Yu, J. Yu, L. Fu, *Mater. Lett.* **2019**, *236*, 412–415.
[46] Y. Xie, F. Gao, X. Tu, X. Ma, Q. Xu, R. Dai, X. Huang, Y. Yu, L. Lu, *J. Electrochem. Soc.* **2019**, *166*, B1673-B1680.
[47] Y. Zhang, X. Jiang, J. Zhang, H. Zhang, Y. Li, *Biosens. Bioelectron.* **2019**, *130*, 315–321.
[48] L. Wu, X. Lu, Dhanjai, Z.-S. Wu, Y. Dong, X. Wang, S. Zheng, J. Chen, *Biosens. Bioelectron.* **2018**, *107*, 69–75.
[49] G. Wang, J. Sun, Y. Yao, X. An, H. Zhang, G. Chu, S. Jiang, Y. Guo, X. Sun, Y. Liu, *Food Analytical Methods* **2020**, *13*, 420–432.
[50] S. Neampet, N. Ruecha, J. Qin, W. Wonsawat, O. Chailapakul, N. Rodthongkum, *Microchim. Acta* **2019**, *186*, 752.
[51] S. S. Shankar, R. M. Shereema, R. B. Rakhi, *ACS Appl. Mater. Interfaces* **2018**, *10*, 43343–43351.
[52] R. Zhang, J. Liu, Y. Li, *ACS Sens.* **2019**, *4*, 2058–2064.
[53] P. A. Rasheed, R. P. Pandey, K. A. Jabbar, J. Ponraj, K. A. Mahmoud, *Anal. Methods* **2019**, *11*, 3851–3856.
[54] R. Huang, S. Chen, J. Yu, X. Jiang, *Ecotoxicol. Environ. Saf.* **2019**, *184*, 109619.
[55] J. Chen, P. Tong, L. Huang, Z. Yu, D. Tang, *Electrochim. Acta* **2019**, *319*, 375–381.
[56] S. Zhou, C. Gu, Z. Li, L. Yang, L. He, M. Wang, X. Huang, N. Zhou, Z. Zhang, *Appl. Surf. Sci.* **2019**, *498*, 143889.
[57] Y. Fang, X. Yang, T. Chen, G. Xu, M. Liu, J. Liu, Y. Xu, *Sens. Actuators B* **2018**, *263*, 400–407.
[58] H. Zhang, Z. Wang, Q. Zhang, F. Wang, Y. Liu, *Biosens. Bioelectron.* **2019**, *124*, 184–190.
[59] X. Chen, J. Li, G. Pan, W. Xu, J. Zhu, D. Zhou, D. Li, C. Chen, G. Lu, H. Song, *Sens. Actuators B* **2019**, *289*, 131–137.
[60] M. Wu, Q. Zhang, Y. Fang, C. Deng, F. Zhou, Y. Zhang, X. Wang, Y. Tang, Y. Wang, *J. Colloid Interface Sci.* **2021**, *586*, 20–29.
[61] H. L. Chia, C. C. Mayorga-Martinez, N. Antonatos, Z. Sofer, J. J. Gonzalez-Julian, R. D. Webster, M. Pumera, *Anal. Chem.* **2020**, *92*, 2452–2459.
[62] M. Song, S.-Y. Pang, F. Guo, M.-C. Wong, J. Hao, *Adv. Sci.* **2020**, *7*, 2001546.
[63] F. Zhao, Y. Yao, C. Jiang, Y. Shao, D. Barceló, Y. Ying, J. Ping, *J. Hazard. Mater.* **2020**, *384*, 121358.
[64] A. Koyappayil, S. G. Chavan, M. Mohammadniaei, A. Go, S. Y. Hwang, M.-H. Lee, *Microchim. Acta* **2020**, *187*, 277.
[65] H. Medetalibeyoglu, M. Beytur, O. Akyıldırım, N. Atar, M. L. Yola, *Sens. Actuators B* **2020**, *319*, 128195.
[66] H. Medetalibeyoglu, G. Kotan, N. Atar, M. L. Yola, *Talanta* **2020**, *220*, 121403.
[67] X. Yang, M. Feng, J. Xia, F. Zhang, Z. Wang, *J. Electroanal. Chem.* **2020**, *878*, 114669.
[68] J. L. Zhang, Y. Li, S. Y. Duan, F. J. He, *Anal. Chim. Acta* **2020**, *1123*, 9–17.
[69] H. Y. Wang, J. J. Sun, L. Lu, X. Yang, J. F. Xia, F. F. Zhang, Z. H. Wang, *Anal. Chim. Acta* **2020**, *1094*, 18–25.
[70] H. Zhang, Z. Wang, F. Wang, Y. Zhang, H. Wang, Y. Liu, *Talanta* **2021**, *224*, 121879.
[71] L. Kashefi-Kheyrabadi, A. Koyappayil, T. Kim, Y.-P. Cheon, M.-H. Lee, *Bioelectrochemistry* **2021**, *137*, 107674.
[72] X. Tu, F. Gao, X. Ma, J. Zou, Y. Yu, M. Li, F. Qu, X. Huang, L. Lu, *J. Hazard. Mater.* **2020**, *396*, 122776.
[73] R. Huang, D. Liao, S. Chen, J. Yu, X. Jiang, *Sens. Actuators B* **2020**, *320*, 128386.
[74] Y. Dang, X. Guan, Y. Zhou, C. Hao, Y. Zhang, S. Chen, Y. Ma, Y. Bai, Y. Gong, Y. Gao, *Sens. Actuators B* **2020**, *319*, 128259.
[75] X. Ma, X. Tu, F. Gao, Y. Xie, X. Huang, C. Fernandez, F. Qu, G. Liu, L. Lu, Y. Yu, *Sens. Actuators B* **2020**, *309*, 127815.
[76] T. Kokulnathan, T. J. Wang, *ACS Appl. Nano Mater.* **2020**, *3*, 2554–2561.
[77] T. Kokulnathan, E. A. Kumar, T.-J. Wang, *ACS Sustainable Chem. Eng.* **2020**, *8*, 12471–12481.
[78] P. K. Kalambate, Dhanjai, A. Sinha, Y. Li, Y. Shen, Y. Huang, *Microchim. Acta* **2020**, *187*, 402.
[79] S. Elumalai, V. Mani, N. Jeromiyas, V. K. Ponnusamy, M. Yoshimura, *Microchim. Acta* **2019**, *187*, 33.
[80] X. Wang, M. Li, S. Yang, J. Shan, *Electrochim. Acta* **2020**, *359*, 136938.
[81] Y. Wang, Z. Zeng, J. Qiao, S. Dong, Q. Liang, S. Shao, *Talanta* **2021**, *221*, 121605.
[82] Y. He, L. Ma, L. Zhou, G. Liu, Y. Jiang, J. Gao, *Nanomaterials* **2020**, *10*, 866.
[83] X. Lv, F. Pei, S. Feng, Y. Wu, S.-M. Chen, Q. Hao, W. Lei, *J. Electrochem. Soc.* **2020**, *167*, 067509.
[84] P. A. Rasheed, R. P. Pandey, T. Gomez, M. Naguib, K. A. Mahmoud, *RSC Adv.* **2020**, *10*, 24697–24704.
[85] E. A. Kumar, T. Kokulnathan, T.-J. Wang, A. J. Anthuvan, Y.-H. Chang, *J. Mol. Liq.* **2020**, *312*, 113354.
[86] Y. Q. Yao, X. H. Han, X. H. Yang, J. Zhao, C. P. Chai, *Chin. J. Chem.* **2021**, *39*, 330–336.
[87] N. Arif, S. Gul, M. Sohail, S. Rizwan, M. Iqbal, *Ceram. Int.* **2021**, *47*, 2388–2396.
[88] L. Shang, X. Wang, W. Zhang, L.-P. Jia, R.-N. Ma, W.-L. Jia, H.-S. Wang, *Sens. Actuators B* **2020**, *325*, 128776.
[89] D. Fang, H. Ren, Y. Huang, H. Dai, D. Huang, Y. Lin, *Sens. Actuators B* **2020**, *312*, 127950.
[90] H. Zhang, Z. Wang, F. Wang, Y. Zhang, H. Wang, Y. Liu, *Anal. Chem.* **2020**, *92*, 5546–5553.
[91] W. Huang, Y. Wang, W.-B. Liang, G.-B. Hu, L.-Y. Yao, Y. Yang, K. Zhou, R. Yuan, D.-R. Xiao, *Anal. Chem.* **2021**, *93*, 1834–1841.
[92] R. A. Soomro, S. Jawaid, N. H. Kalawar, M. Tunesi, S. Karakuş, A. Kilislioğlu, M. Willander, *Biosens. Bioelectron.* **2020**, *166*, 112439.
[93] F. Han, Z. Song, J. Xu, M. Dai, S. Luo, D. Han, L. Niu, Z. Wang, *Biosens. Bioelectron.* **2021**, *177*, 112978–112978.
[94] R. A. Soomro, S. Jawaid, P. Zhang, X. Han, K. R. Hallam, S. Karakuş, A. Kilislioğlu, B. Xu, M. Willander, *Sens. Actuators B* **2021**, *328*, 129074.
[95] C. Yuan, Z. He, Q. Chen, X. Wang, C. Zhai, M. Zhu, *Appl. Surf. Sci.* **2021**, *539*, 148241.
[96] Q. Q. Jiang, H. J. Wang, X. Q. Wei, Y. Wu, W. L. Gu, L. Y. Hu, C. Z. Zhu, *Anal. Chim. Acta* **2020**, *1119*, 11–17.
[97] M. Sharifuzzaman, S. C. Barman, M. A. Zahed, S. Sharma, H. Yoon, J. S. Nah, H. Kim, J. Y. Park, *Small* **2020**, *16*, 2002517.
[98] Y. Yao, L. Lan, X. Liu, Y. Ying, J. Ping, *Biosens. Bioelectron.* **2020**, *148*, 111799.
[99] S. F. Zhao, F. X. Hu, Z. Z. Shi, J. J. Fu, Y. Chen, F. Y. Dai, C. X. Guo, C. M. Li, *Nano Res.* **2021**, *14*, 879–886.

[100] S. Zhang, M. A. Zahed, M. Sharifuzzaman, S. Yoon, X. Hui, S. Chandra Barman, S. Sharma, H. S. Yoon, C. Park, J. Y. Park, *Biosens. Bioelectron.* **2021**, *175*, 112844–112844.
[101] M. Mohammadniaei, A. Koyappayil, Y. Sun, J. Min, M.-H. Lee, *Biosens. Bioelectron.* **2020**, *159*, 112208.
[102] M. Li, L. Wang, R. Liu, J. Li, Q. Zhang, G. Shi, Y. Li, C. Hou, H. Wang, *Biosens. Bioelectron.* **2021**, *174*, 112828.
[103] L. Y. Zhou, X. Zhang, L. Ma, J. Gao, Y. J. Jiang, *Biochem. Eng. J.* **2017**, *128*, 243–249.
[104] L. X. Wu, X. B. Lu, Dhanjai, Z. S. Wu, Y. F. Dong, X. H. Wang, S. H. Zheng, J. P. Chen, *Biosens. Bioelectron.* **2018**, *107*, 69–75.
[105] F. Wang, C. Yang, M. Duan, Y. Tang, J. Zhu, *Biosens. Bioelectron.* **2015**, *74*, 1022–1028.
[106] Y. J. Jiang, X. N. Zhang, L. J. Pei, S. Yue, L. Ma, L. Y. Zhou, Z. H. Huang, Y. He, J. Gao, *Chem. Eng. J.* **2018**, *339*, 547–556.
[107] G. X. Wang, J. F. Sun, Y. Yao, X. S. An, H. Zhang, G. L. Chu, S. Jiang, Y. M. Guo, X. Sun, Y. Liu, *Food Anal. Meth.* **2020**, *13*, 420–432.
[108] J. L. Chen, P. Tong, L. T. Huang, Z. H. Yu, D. P. Tang, *Electrochim. Acta* **2019**, *319*, 375–381.
[109] a) S. Ranallo, A. Porchetta, F. Ricci, *Anal. Chem.* **2019**, *91*, 44–59; b) S. Lv, K. Zhang, L. Zhu, D. Tang, *Anal. Chem.* **2020**, *92*, 1470–1476; c) R. Zeng, Z. Luo, L. Su, L. Zhang, D. Tang, R. Niessner, D. Knopp, *Anal. Chem.* **2019**, *91*, 2447–2454; d) K. Zhang, S. Lv, Q. Zhou, D. Tang, *Sens. Actuators B* **2020**, *307*, 127631.
[110] A. Abi, Z. Mohammadpour, X. Zuo, A. Safavi, *Biosens. Bioelectron.* **2018**, *102*, 479–489.
[111] D. H. Wu, M. Y. Wu, J. H. Yang, H. W. Zhang, K. F. Xie, C. T. Lin, A. M. Yu, J. H. Yu, L. Fu, *Mater. Lett.* **2019**, *236*, 412–415.
[112] F. Shahzad, A. Iqbal, S. A. Zaidi, S. W. Hwang, C. M. Koo, *J. Ind. Eng. Chem.* **2019**, *79*, 338–344.
[113] T. S. H. Pham, L. Fu, P. Mahon, G. Lai, A. Yu, *Electrocatalysis* **2016**, *7*, 411–419.
[114] Y. Zhang, X. T. Jiang, J. J. Zhang, H. Zhang, Y. C. Li, *Biosens. Bioelectron.* **2019**, *130*, 315–321.
[115] H. Y. Zou, F. F. Zhang, H. Y. Wang, J. F. Xia, L. N. Gao, Z. H. Wang, *New J. Chem.* **2019**, *43*, 2464–2470.
[116] R. Y. Zhang, J. Liu, Y. C. Li, *ACS Sens.* **2019**, *4*, 2058–2064.
[117] P. Abdul Rasheed, R. P. Pandey, T. Gomez, K. A. Jabbar, K. Prenger, M. Naguib, B. Aïssa, K. A. Mahmoud, *Electrochem. Commun.* **2020**, *119*, 106811.
[118] Y. F. Fang, X. C. Yang, T. Chen, G. F. Xu, M. L. Liu, J. Q. Liu, Y. H. Xu, *Sens. Actuators B* **2018**, *263*, 400–407.
[119] H. X. Zhang, Z. H. Wang, Q. X. Zhang, F. Wang, Y. Liu, *Biosens. Bioelectron.* **2019**, *124*, 184–190.
[120] X. Chen, J. Li, G. C. Pan, W. Xu, J. Y. Zhu, D. L. Zhou, D. Y. Li, C. Chen, G. Y. Lu, H. W. Song, *Sens. Actuators B* **2019**, *289*, 131–137.
[121] a) Z. Yu, G. Cai, X. Liu, D. Tang, *ACS Appl. Mater. Interfaces* **2020**, *12*, 40133–40140; b) Z. Yu, G. Cai, X. Liu, D. Tang, *Anal. Chem.* **2021**, *93*, 2916–2925; c) Z. Yu, G. Cai, P. Tong, D. Tang, *ACS Sens.* **2019**, *4*, 2272–2276; d) Z. Yu, Y. Tang, G. Cai, R. Ren, D. Tang, *Anal. Chem.* **2019**, *91*, 1222–1226.

Received: May 14, 2021
Accepted: May 17, 2021
Published online on June 2, 2021

